DIFFUSIOPHORESIS AND OSMOTIC DIFFUSION IN TERNARY AQUEOUS MIXTURES OF POLYETHYLENE GLYCOL CONTAINING TRIMETHYLAMINE-N-OXIDE OR UREA AS COSOLUTES

by

Lara Richelle Lechlitner

Bachelor of Science, 2011
Tarleton State University
Stephenville, TX

Submitted to the Graduate Faculty of the
College of Science and Engineering
Texas Christian University
in partial fulfillment of the requirements
for the degree of

Master of Science

May, 2017

DIFFUSIOPHORESIS AND OSMOTIC DIFFUSION IN

TERNARY AQUEOUS MIXTURES OF POLYETHYLENE GLYCOL CONTAINING

TRIMETHYLAMINE-N-OXIDE OR UREA AS COSOLUTES

by

Lara Lechlitner

Dissertation approved:

4/28/2017

Major Professor

Benjamin G Jarvey 4/28/2017

4/28/2017

For the College of Science and Engineering

ACKNOWLEDGEMENTS

I would like to express my deepest appreciation to Dr. Onofrio Annunnziata. He is one of the most talented and knowledgeable scientists I know. He has been a truly gracious supporter throughout my journey at TCU.

Next, I would like to thank my other committee members: Dr. Sergei Dzyuba and Dr. Benjamim Janesko. I greatly appreciate their time, support, challenging questions and insights throughout my time at TCU and while working on my thesis.

I must also thank my mentors from the past: Dr. Gerald Springer and Dr. Reuben Walter. I want to express my appreciation to others, who have helped me at TCU: Jerry, Dave, Page, Pam, and Carolyn.

Most importantly, I would like to acknowledge my family and friends for their support and understanding throughout this process. My husband and best friend, John, he has been a constant encourager, never wavering in his confidence in what I can accomplish. I want to thank my father and mother for the example they set in scholastics. I want to give special thanks, to my grandmother and sister for always being my biggest fans no matter what happens. Finally, I want to express my gratitude to Dr. Viviana Costa, Marlius Castillo, and Aisha Fahim for their friendship and scientifically insightful conversations.

TABLE OF CONTENTS

LIST OF FIGURES

LIST OF TABLES

Chapter 1

Motivation

1.1 Introduction

A concentration gradient of a solute within a liquid mixture induces the net transport of solute molecules from high to low concentration. This transport phenomenon is denoted as diffusion. Diffusion-based transport in liquids is important in separation technologies, phase transitions, surface adsorption, controlled-release technologies, microfluidics and biochemical systems.[1-6] Accurate descriptions of the diffusion processes are a necessary step towards understanding the dynamics within liquid mixtures, improving existing technologies and developing better ones. In most mass-transport problems, diffusion occurs within multicomponent liquid systems; *i.e.*, those mixtures that contain more than one solute component. One aspect of diffusion in multicomponent systems that is not well understood is cross-diffusion. This is the diffusion of a solute induced by the concentration gradient of another solute.[1-6]

The diffusion of macromolecules in solutions is a particular area of interest relevant to the applications listed above.[1-7] Indeed, there are many studies focusing on the diffusion of proteins and synthetic polymers in aqueous and non-aqueous mixtures.[1,8,9-13] Related transport parameters (Brownian mobilities) have been used to characterize the size of macromolecules and their aggregates and model diffusion rates, relevant to the kinetics of (bio)chemical processes, phase transitions and diffusion-based controlled release.[10,14] However, often the investigated systems not only contain the macromolecule of interest but also other solutes (cosolutes), and cross-diffusion may occur. Nonetheless, cross-diffusion mechanisms are often ignored in these studies, mainly because cross-diffusion data are scarce and very difficult to measure.

A concentration gradient of a cosolute can induce the diffusion of macromolecules or colloidal particles.[1,7,15-17] This specific cross-diffusion mechanism is denoted as diffusiophoresis.[1-7] The origin of this name may be better appreciated by considering another well-known transport phenomenon denoted as electrophoresis. Electrophoresis describes the net transport of macromolecules induced by a gradient of electrical potential, while diffusiophoresis describes the net transport of macromolecules (or colloidal particles) induced by a gradient of solute concentration (a gradient of chemical potential rigorously).[1,4,8]

Recently, there has been a growing interest on the use of microfluidics as a means to achieve separation of macromolecules (*e.g.*, proteins) on the microscale level for applications such as high-throughput screening.[4,18] The effects of diffusiophoresis have been also investigated inside microfluidic devices.[4,18] Specifically, it has been shown that cosolute concentration gradients result in large shifts of colloidal particles. [1,8,15-18] In other words, the effect of a cosolute concentration gradient on a (neutral or charged) macromolecule (diffusiophoresis) resembles to that of an electrical-potential gradient on a charged macromolecule (electrophoresis).[13] Thus, these studies have shown that cosolute concentration gradients may be used to direct the motion of macromolecules. [1,8,15-18]

The separation of colloidal particles in microfluidic systems based on electrophoresis has been demonstrated. However, Joule heating effects have been observed in related experiments.[19] Thus, the extension of microfluidic-based electrophoresis to more labile macromolecules is limited by their fragility at the small-scale level.[19] Because cosolute concentration gradients can be less invasive than external electric fields and microfluidics devices have been successfully employed to set up cosolute concentration gradients, it becomes important to develop novel separation techniques based on diffusiophoresis. [1,16,17,19] Cosolute concentration gradients could

be employed to separate two distinct macromolecules relevant to separation technologies, focus macromolecules within a narrow spatial domain relevant to self-assembly, and direct and boost the motion of macromolecules towards solid surfaces, relevant to adsorption, crystal growth and sensor technologies. [1,8,15-14] All these applications require a fundamental understanding of cross-diffusion transport in multicomponent mixtures containing macromolecules.

Nearly all research studies on cosolute-induced diffusiophoresis have pertained to aqueous univalent chloride salts (NaCl and KCl) at low salt concentration ($\approx 0.1\ \mathrm{mol \cdot dm^{-3}}$ or less) in solution with large (≈100 nm) particles.[1,8,15,16,20-21] Recently, we have employed Rayleigh interferometry to show that diffusiophoresis occurs also in the instance of macromolecules such as proteins and polymers in aqueous salt mixtures.[1,8-10,17, 23-25] In these studies, diffusiophoresis measurements were also performed at relatively high salt concentrations ($\approx 1\ \mathrm{mol \cdot dm^{-3}}$ or higher).[1,8-10]

In relation to salts, there is an extensive literature on their application as promotors of precipitation and crystallization of macromolecules, especially in the case of proteins.[1,3-5] Furthermore, salts have been ranked in the Hofmeister series according to their thermodynamic effectiveness in inducing protein precipitation.[1,8] In this series, sulfates are regarded as the most effective precipitating agents (salting-out agents), while, on the other hand, thiocyanates are regarded as solubility enhancers (salting-in agents). [1,8] Such behavior is not only observed for proteins but also for synthetic polymers in water. We have shown that the magnitude of salt-induced macromolecule diffusiophoresis also follow the Hofmeister series. [1,8] Indeed, concentration gradients of sodium sulfate can be used to produce large diffusiophoresis effects.[1,8] In most of these studies, polyethylene glycol (PEG) was selected as the model macromolecule. This synthetic polymer was chosen because it is neutral and highly soluble (hydrophilic) in water

at room temperature. Contrary to (charged) proteins, the effect of salts on PEG does not involve electrostatic ionic interactions. Thus, PEG-salt net interactions in water depend only on the hydration properties of the macromolecule and salt ions.[1,8] PEG is commercially available in many molecular weights. Diffusiophoresis studies as a function of PEG molecular weight has allowed us to experimentally determine how diffusiophoresis compares to polymer Brownian mobility as the polymer size increases.[10,23] PEG also has a broad spectrum of pharmaceutical and industrial applications due to its non-toxic character. Indeed, PEG has been used as a biomaterial for cell and tissue engineering, coating of implants, biosensors and drug delivery systems.[26-29]

Our studies on salt-induced diffusiophoresis have also shown the importance of another distinct cross-diffusion mechanism, we denoted as salt osmotic diffusion.[1,8,17] This is the diffusion of salt induced by a concentration gradient of macromolecules. As in the case of diffusiophoresis, the magnitude of salt osmotic diffusion also follows the Hofmeister series.[1,8] These studies have also allowed us to realize that the examination of salt osmotic diffusion data represented a needed step for understanding macromolecule diffusiophoresis. [1,8,22] Specifically, we have shown that diffusiophoresis is a function of a kinetic and a thermodynamic parameter. To identify the relative contribution of these two parameters, osmotic-diffusion data were also needed.

All these studies showed that salt-induced diffusiophoresis of macromolecules relates to the thermodynamic effectiveness of salts in precipitating macromolecules from aqueous solutions.[1,8] Interestingly, it is known that the thermodynamic properties of macromolecules can be also influenced by neutral cosolutes.[30-34] In the case of proteins, it is known that the thermodynamic effect of trimethylamine-N-oxide (TMAO) is similar to that of salting-out agent such as sodium sulfate, while that of urea is similar to that of salting-in agent such as sodium thiocyanate.[33]

TMAO and urea are known as osmolyte and denaturant, respectively. Interestingly, these two neutral organic molecules can also be found in living systems at relatively high concentrations. TMAO and other osmolytes are known to significantly lower the water chemical potential. Thus, in the presence of TMAO, a living cell is capable of fighting against dehydration. Specifically, TMAO thermodynamically hinders the water osmotic flow from the cell interiors to cell surroundings. In other words, cells can maintain their volume under conditions of osmotic stresses.

Urea is a byproduct of protein degradation inside living systems. Urea has a broad spectrum of industrial applications. It is employed as a fertilizer and is also an ingredient found in cosmetic and pharmaceutical formulations. Urea is a denaturant because it is known to thermodynamically destabilize the native conformation of proteins. Thus urea is extensively used to characterize the thermodynamic stability of proteins in biochemical and biophysical laboratory experiments. It is interesting to observe that TMAO, on the other hand, is known for its ability to stabilize the native conformation of proteins. Thus, in the presence of TMAO, the denaturing effect of urea on proteins inside living systems is significantly reduced.[34]

The goal of this thesis is to investigate TMAO-induced and urea-induced diffusiophoresis of PEG. TMAO and urea osmotic diffusion will be also characterized. Specifically, we will experimentally characterize diffusion coefficients in ternary PEG-TMAO-water and PEG-urea-water systems at 25 ºC using Rayleigh interferometry. These data will be then used to determine PEG diffusiophoresis coefficients and cosolute osmotic diffusion coefficients as a function of cosolute concentration. Our experimental results will be then theoretically examined within the framework of non-equilibrium thermodynamics.

1.2 The Molecular Structures of PEG, TMAO and urea

The chemical structure of PEG is shown in Fig. 1.1. In our studies, PEG has a molecular weight of 20 kg mol^{-1}. This corresponds to about 450 monomeric units. This linear flexible polymer exhibits a coil-like conformation in water at room temperature. Since this polymer is hydrophilic, PEG coils tend to have a slightly more swollen conformation in water compared to that predicted from a random coil.

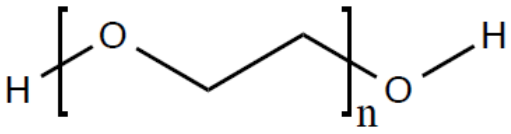

Figure 1.1: Structure of Polyethylene Glycol, with n being the number of repeating units.

The chemical structure of TMAO is shown in Fig. 1.2. Note that this neutral molecule is a zwitterion with a positive charge located on the N atom and a negative charge located on the O atom. The TMAO molecule has an sp^3 hybridized nitrogen atom.

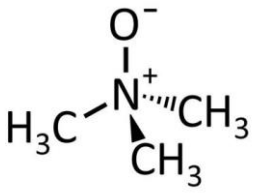

Figure 1.2: Structure of TMAO

The chemical structure of urea is shown in Fig. 1.3. The urea molecule is planar with respect to the carbon being described as sp^2 hybridized. The nitrogen atoms are sp^3 hybridized or tetrahedral. Note that the C-N bonds have significant double bond character due to resonance.

Urea is highly soluble in aqueous solutions due to its ability to engage in extensive hydrogen bonding with water.

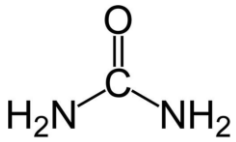

Figure 1.3: Structure of Urea

Chapter 2

Theoretical Background

2.1 Diffusion coefficient

In a binary solute(1)-solvent(0) mixture, diffusion is the transport phenomenon that describes the net motion of solute particles from high to low solute concentration in the absence of external fields. To examine diffusion and introduce the diffusion coefficient, we consider the limiting case of an ideal-dilute solution. This corresponds to non-interacting solute particles. We then consider the forces that apply to the solute particles in isothermal conditions. If the particles are overall moving with constant drift speed, v, the net driving force, F, must be equal to a frictional force, fv, where f is a frictional coefficient. Note that both F and v are vectors sharing the same direction in isotropic liquids. The drift speed of the solute particles is therefore given by[17]

$$\vec{v} = \frac{\vec{F}}{f} \tag{2.1}$$

For diffusion, the driving force is the gradient of solute chemical potential, μ_1. In the limit of infinite dilution, we can write at constant temperature:

$$\vec{F} = -\frac{\nabla \mu_1}{N_A} = -\frac{k_B T}{C_1} \nabla C_1 \tag{2.2}$$

where $\nabla \equiv (\partial/\partial x, \partial/\partial y, \partial/\partial z)$, N_A is the Avogadro's number, k_B the Boltzmann constant, C_1 is the solute molar concentration and T the absolute temperature. After inserting Eq. 2.2 into Eq. 2.1, we obtain:

$$-J_1 = \frac{k_B T}{f} \nabla C_1 \tag{2.3}$$

where $J_1 = C_1 v$ is the net flux of solute particles from high to low solute concentration.[4]

The tracer diffusion coefficient of the solute particles, D_1^0 (units, $\mathrm{m}^2 \cdot \mathrm{s}^{-1}$), can be introduced as

$$D_1^0 = \frac{k_B T}{f} \tag{2.4}$$

Equation 2.4 is known as Einstein equation and provides the basis of the Brownian motion theory. [35] The diffusion coefficient, D_1^0, is also denoted as Brownian mobility. Note that D_1^0 is the ratio of the thermal energy term, $k_B T$, responsible for particle motion and the opposing friction caused by the surrounding fluid (solvent). The higher the temperature the faster particles move. The larger the friction coefficient the slower the particles diffuse. The value of f is related to the size and shape of the solute particles, and the viscosity, η (units, $\mathrm{kg} \cdot \mathrm{m}^{-1}\mathrm{s}^{-1}$), of the surrounding medium (solvent) assumed as a continuum. For a spherical solute particle, it can be shown that $f = 6\pi\eta R_h$ (Stokes' law), where R_h is the radius of the particle (hydrodynamic radius).[36] This relation is usually extended also to non-spherical particles with the understanding that R_h is the equivalent hydrodynamic radius of a sphere. Equation 2.3 can be therefore rewritten in the following way:

$$D_1^0 = \frac{k_B T}{6\pi\eta R_h} \tag{2.5}$$

Equation 2.5 is known as the Stokes-Einstein equation. This equation is important because it shows that the diffusion coefficient of a macromolecule is expected to be significantly smaller than that of a co-solute with relatively low molecular weight. Equation 2.4 also shows that the diffusion coefficient of a solute is inversely proportional to the viscosity of the surrounding medium.

2.2 Fick's Law

Equation 2.4 can be extended to any arbitrary solute concentration, provided that $D_1^0 = k_B T / f$ is replaced by $D_1(C_1)$, a phenomenological transport parameter denoted as the mutual diffusion coefficient. The adjective "mutual" is introduced to emphasize that D_1 also describes the compensating diffusion of solvent molecules occurring in the opposite direction of solute diffusion. The generalization of Eq. 2.4 to finite solute concentrations in binary solute(1)-solvent(0) systems is known as Fick's law:[37]

$$-J_1 = D_1 \nabla C_1 \tag{2.6}$$

The generalization of Eq. 2.6 can be extended to multicomponent systems. For a ternary solute(1)-solute(2)-solvent(0) system, we have the following matrix:

$$-\begin{bmatrix} J_1 \\ J_2 \end{bmatrix} = \begin{bmatrix} D_{11} & D_{12} \\ D_{21} & D_{22} \end{bmatrix} \begin{bmatrix} \nabla C_1 \\ \nabla C_2 \end{bmatrix} \tag{2.7}$$

where C_1 and C_2 are the molar concentrations of solute 1 and solute 2, and J_1 and J_2 are the corresponding molar fluxes. The four D_{ij} (with $i, j = 1, 2$), which are represented as a 2×2 diffusion-coefficient matrix, are denoted as ternary diffusion coefficients. In this thesis, solute 1 and solute 2 are the macromolecule (PEG) and cosolute (TMAO or urea) components, respectively. The diffusion coefficients, D_{11} and D_{22}, describe the flux of macromolecule and cosolute due to their own solute concentrations. These two coefficients are expected to be closely related to the corresponding binary diffusion coefficients, D_1 and D_2, associated with the macromolecule-solvent and cosolute-solvent systems, respectively. The off-diagonal diffusion coefficients, D_{12} and D_{21}, are denoted as cross-diffusion coefficients, with D_{12} describing the

flux of macromolecule due to the concentration gradient of the cosolute, and D_{21} describing the flux of cosolute due to the concentration gradient of the macromolecule. The cross-terms D_{12} and D_{21} will be related to macromolecule diffusiophoresis and cosolute osmotic diffusion, respectively.

2.3 Diffusion and Non-equilibrium Thermodynamics

Non-equilibrium thermodynamics provides the theoretical basis for understanding diffusion transport in multicomponent systems. We shall see that ternary diffusion coefficients are linear combinations of fundamental thermodynamic and transport parameters. Before we derive these important relationships, we need to introduce the concept of reference frame. Diffusion coefficients can be reported in different reference frames.[38] In the volume-fixed frame, the fluxes of the components of a ternary system fulfill the condition: $(J_0)_{\mathrm{V}}\bar{V}_0 + (J_1)_{\mathrm{V}}\bar{V}_1 + (J_2)_{\mathrm{V}}\bar{V}_2 = 0$; in the solvent-fixed frame, we have $(J_0)_0 = 0$. Here, J_i and $\bar{V}_i$ are the molar flux and partial molar volume of component *i*, respectively. The subscript "V" denotes the volume-fixed frame. The subscript "0" denotes the solvent component when added directly to a flux, and denotes the solvent-fixed frame when added outside the parentheses to an already-subscripted flux or diffusion coefficient. We note that volume-fixed frame diffusion coefficients are obtained experimentally.[23] However, solvent-fixed frame diffusion coefficients are more directly related to the thermodynamics of mixtures. The solvent-fixed frame coefficients, $(D_{ij})_0$, are related to the volume-fixed frame coefficients $(D_{ij})_{\mathrm{V}}$ by the following relations:[39,40]

$$(D_{11})_0 = (D_{11})_V + [C_1/(1-C_1\bar{V}_1 - C_2\bar{V}_2)]\ [\bar{V}_1(D_{11})_V + \bar{V}_2(D_{21})_V] \quad (2.8.1)$$

$$(D_{12})_0 = (D_{12})_V + [C_1/(1-C_1\bar{V}_1 - C_2\bar{V}_2)]\ [\bar{V}_1(D_{12})_V + \bar{V}_2(D_{22})_V] \quad (2.8.2)$$

$$(D_{21})_0 = (D_{21})_V + [C_2/(1-C_1\bar{V}_1 - C_2\bar{V}_2)]\ [\bar{V}_1(D_{11})_V + \bar{V}_2(D_{21})_V] \quad (2.8.3)$$

$$(D_{22})_0 = (D_{22})_V + [C_2/(1-C_1\bar{V}_1 - C_2\bar{V}_2)]\ [\bar{V}_1(D_{12})_V + \bar{V}_2(D_{22})_V] \quad (2.8.4)$$

Non-equilibrium thermodynamics describes isothermal diffusion transport in the solvent-fixed reference frame. [15,16,20] In the following analysis, we will omit subscripts "0" for the solvent-fixed reference frame in order to simplify notation. For a binary solute(1)-solvent(0) system, we have:

$$-J_1 = L_{11}\nabla\mu_1 \quad (2.9)$$

where the L_{11} term is a fundamental transport parameter known as the Onsager transport coefficient.[4,9] Note that Eq. 2.9 is a linear law consistent with Fick's law but emphasizes that the chemical-potential gradient not the concentration gradient is the actual driving force for diffusion. If we combine Eqs. 2.6 with 2.9, we obtain:

$$D_1 = L_{11}\,\mu_{11} \quad (2.10)$$

where $\mu_{11} \equiv (\partial\mu_1/\partial C_1)_{T,p}$, a molarity-based chemical-potential derivative, is a parameter characterizing the thermodynamic properties of the binary solution.[4,9] Eq. 2.2 shows that the observed diffusion coefficient is the product of a transport parameter and a thermodynamic parameter. In the limit of infinite dilution, we know that $(\partial\mu_1/\partial C_1)_{T,p} = RT/C_1$. In this limit, we obtain:

$$D_1^0 = \frac{RT\,L_{11}}{C_1} \quad (2.11)$$

The extension of Eq. 2.9 to ternary systems is:

$$-\begin{bmatrix} J_1 \\ J_2 \end{bmatrix} = \begin{bmatrix} L_{11} & L_{12} \\ L_{21} & L_{22} \end{bmatrix} \begin{bmatrix} \nabla\mu_1 \\ \nabla\mu_2 \end{bmatrix} \tag{2.12}$$

where the four L_{ij} (with $i, j = 1, 2$) terms represent a 2×2 matrix of Onsager transport coefficients. Note that this matrix is symmetric with $L_{12} = L_{21}$ being the Onsager Reciprocal Relation.[41,42] If we combine Eqs. 2.7 with 2.12, we obtain:

$$(D_{11})_0 = (L_{11})_0 \mu_{11} + (L_{12})_0 \mu_{21} \tag{2.13.1}$$

$$(D_{12})_0 = (L_{11})_0 \mu_{12} + (L_{12})_0 \mu_{22} \tag{2.13.2}$$

$$(D_{21})_0 = (L_{21})_0 \mu_{11} + (L_{22})_0 \mu_{21} \tag{2.13.3}$$

$$(D_{22})_0 = (L_{21})_0 \mu_{12} + (L_{22})_0 \mu_{22} \tag{2.13.4}$$

where $\mu_{ij} \equiv (\partial\mu_i / \partial C_j)_{T,p,C_k,k\neq j}$ (with $i, j, k = 1, 2$) are parameters characterizing the thermodynamic properties of the ternary mixture.

2.4 Polymer Diffusiophoresis and Cosolute Osmotic Diffusion

To describe polymer diffusiophoresis and cosolute osmotic diffusion, the two following reduced parameters are defined:

$$\hat{D}_{12} \equiv \lim_{C_1 \to 0}[C_2 D_{12} / (2C_1 y_2 D_{\mathrm{p}})] \qquad \text{for polymer diffusiophoresis} \tag{2.14.1}$$

$$\hat{D}_{21} \equiv \lim_{C_1 \to 0}[D_{21} / D_{22}] \qquad \text{for cosolute osmotic diffusion} \tag{2.14.2}$$

where D_{p} is the macromolecule tracer-diffusion coefficient (D_1^0 in Section 2.1), characterizing polymer Brownian mobility in aqueous solution at infinite dilution.[9] The factor $y_2 \equiv (1 + d\ln f_2 / d\ln C_2)$ in Eq. 2.14 is a thermodynamic factor of the binary cosolute-water system, with f_2 being the corresponding activity coefficient of the cosolute.[9] Note that both D_{p}

and y_2 are functions of cosolute concentration, C_2. Values of $y_2(C_2)$ are available through the literature.[57,60] Values of $D_{\mathrm{p}}(C_2)$ can be obtained from the known value of $D_{\mathrm{p}}(0)$ in water and data of relative viscosity of of the binary cosolute-water system, $\eta_r\left(C_2\right)$ can be used to characterize $D_{\mathrm{p}}\left(C_2\right)=D_{\mathrm{p}}(0)/\eta_r\left(C_2\right)$ based on the Stokes-Einstein equation. In Eqs. 2.14.1 and 2.14.2 the experimental values of the diffusion-coefficient matrix D_{ij} (in the solvent-fixed reference frame) are needed to calculate $\hat{D}_{12}$ and $\hat{D}_{21}$.

In order to provide a theoretical interpretation on $\hat{D}_{12}$ and $\hat{D}_{21}$, we link these two normalized parameters to the Onsager transport coefficients and thermodynamic parameters in Eq. 2.12. According to Eqs. 2.13.2 and 2.13.3 we can write:

$$\frac{D_{12}}{L_{11}\mu_{22}}=\frac{\mu_{12}}{\mu_{22}}+\frac{L_{12}}{L_{11}} \tag{2.15.1}$$

$$\frac{D_{21}}{L_{22}\mu_{22}}=\frac{\mu_{21}}{\mu_{22}}+\frac{L_{21}}{L_{11}}\frac{L_{11}}{L_{22}}\frac{\mu_{11}}{\mu_{22}} \tag{2.15.2}$$

In the limit of $C_1\to 0$, we know that $L_{11}\mu_{22}=D_{\mathrm{p}}(y_2\,C_1/C_2)$ and $L_{22}\mu_{22}=D_{22}=D_2$. Thus, the left side of Eqs. 2.15.1 and 2.15.2 become $\hat{D}_{12}$ and $\hat{D}_{21}$, respectively.[9] Furthermore, $L_{11}\mu_{11}=D_{\mathrm{p}}$ and $(L_{11}\mu_{11})/(L_{22}\mu_{22})=D_{\mathrm{P}}/D_2$ in Eq. 2.15.2. In relation to Eq. 2.15.1, it is convenient to introduce the following thermodynamic and kinetic parameters:[23,24,63]

$$\gamma\equiv\lim_{C_1\to 0}\frac{\mu_{12}}{\mu_{22}} \tag{2.16}$$

$$\lambda\equiv-\lim_{C_1\to 0}\frac{L_{12}}{L_{11}} \tag{2.17}$$

In previous studies, we have shown that the magnitude of γ is comparable with that of λ.[1] By using Eq. 2.15.2 and remember the ORR, we obtain:

$$\hat{D}_{12} = \gamma - \lambda \tag{2.18.1}$$

$$\hat{D}_{21} = \gamma + \bar{V}_1 C_2 - \alpha\ \lambda \tag{2.18.2}$$

where $\alpha \equiv D_P / D_2$ and we have used $\mu_{21} / \mu_{22} = \gamma + C_2 \bar{V}_1$.[9] This expression of μ_{21} / μ_{22} will be discussed in Section 2.3. The value of α is small for polymers in the presence of low-molecular weight cosolutes due to the relative large size of polymers (typically $\alpha < 0.05$). As shown by Eq. 2.18, polymer diffusiophoresis equally depends on both the thermodynamic and transport parameters. On the other hand, $\alpha\lambda$ in Eq. 2.18.2 represents a kinetic relatively small correction. This implies that $\hat{D}_{21}$ is approximately a thermodynamic parameter. If the partial molar volume of the polymer, $\bar{V}_1$, is known, measurements of $\hat{D}_{21}$ as a function of cosolute concentration allows us to extract the thermodynamic parameter $\gamma(C_2)$. Thus, measurements of $\hat{D}_{12}$ as a function of cosolute concentration will then allow us to extract the kinetic parameter $\lambda(C_2)$. We can also appreciate that the examination of $\hat{D}_{21}(C_2)$ (co-solute osmotic diffusion) represents a prerequisite for understanding the behavior of $\hat{D}_{12}(C_2)$ (polymer diffusiophoresis).

In order to provide a physical interpretation on $\hat{D}_{12}$ and $\hat{D}_{21}$, we link these normalized parameters to macromolecular transport and equilibrium dialysis, respectively. The parameter $\hat{D}_{12}$ describes the effect of the cosolute chemical field ($\nabla\mu_2$) on the net migration rate of a polymer, r_P:[1]

$$r_P = -D_P\left(\nabla \ln C_1 + \hat{D}_{12}\frac{\nabla\mu_2}{RT}\right) \tag{2.19}$$

where we have used $r_P = J_1 / C_1$. Eq. 2.19 is obtained after differentiating $\mu_1(C_1, \mu_2)$ in Eq. 2.12 in the limit of $C_1 \to 0$, and then using the definitions of γ and λ. Interestingly, this equation

for diffusiophoresis is analogous to the electrokinetic equation describing electrophoresis in the presence of an electrical field.[63]

The parameter $\hat{D}_{21}$ is related to cosolute equilibrium partitioning in equilibrium dialysis. In the hypothetical limit of the mobility of the macromolecule being infinitely slow compared to that of the cosolute ($\alpha \to 0$), the co-solute component reaches equilibrium ($\nabla \mu_2 = 0$) in the presence of an infinitely slower dissipating macromolecule concentration gradient. This implies that $J_2 = 0$. According to Fick's law ($-J_2 = D_{21}\nabla C_1 + D_{22}\nabla C_2$), we deduce that $D_{21}/D_{22} = -\nabla C_2 / \nabla C_1$ in this limit. We can therefore write:

$$\left(\frac{\partial C_2}{\partial C_1}\right)_{\mu_2} = -\lim_{\alpha \to 0} \hat{D}_{21} \tag{2.20}$$

The parameter $(\partial C_2 / \partial C_1)_{\mu_2}$, which characterizes the difference in cosolute concentration between two solutions of different macromolecule concentration at equilibrium, describes cosolute partitioning across a membrane not permeable to the polymer component. Since polymers are not infinitely slow, the small kinetic correction, $\alpha\lambda$ in Eq. 2.18.2 characterizes the deviation of the experimental $\hat{D}_{21}$ from the hypothetical $\lim_{\alpha \to 0} \hat{D}_{21}$.

In summary, we have introduced two normalized parameters, $\hat{D}_{12}$ and $\hat{D}_{21}$, describing polymer diffusiophoresis and cosolute osmotic diffusion, respectively. The fist parameter describes the effect of cosolute chemical fields on the net migration rate of polymer, while the second parameter is closely related to co-solute partitioning in equilibrium dialysis. We have also theoretically connected $\hat{D}_{12}$ and $\hat{D}_{21}$ to two fundamental thermodynamic and kinetic parameters, γ and λ. These two parameters will be further discussed in the following remaining sections.

2.5 Examination of the thermodynamic parameter, γ

The isobaric and isothermal effect of cosolutes on the thermodynamic stability of macromolecules is related to macromolecule(1)-cosolute(2) net interactions in water(0). In general, the thermodynamic properties of ternary mixtures is described by the four chemical-pontential derivatives, $\mu_{ij} \equiv (\partial \mu_i / \partial C_j)_{C_k, k \neq j}$, which were introduced in Section 2.4. In our case, we have $\mu_{11} = RT / C_1$ and $\mu_{22} = RT\, y_2 / C_2$ (in the limit of $C_1 \to 0$). The effect of cosolute on macromolecule is described by the chemical-potential cross derivative μ_{12}. A positive value of μ_{12} implies that the chemical potential of the macromolecule, μ_1, increases as the cosolute concentration, C_2, increases. In contrast, a negative value of μ_{12} implies that μ_1, decreases as C_2 increases. A cosolute-induced increase (decrease) in the macromolecule chemical potential implies that the macromolecule-cosolute net interactions are repulsive (attractive) in water. In the presence of net repulsive interactions, a macromolecule tends to minimize its interactions with the surrounding cosolute by either collapsing on itself (e.g., favoring compact conformational states) or phase separating from the aqueous solution. In the presence of net attractive interactions, a macromolecule tends to maximize its interactions with the cosolute leading to cosolute binding (e.g., host-guest interactions). The other chemical-potential cross derivative, μ_{21}, is linked to μ_{12} by a Maxwell relation. In the limit of $C_1 \to 0$, we have:

$$\frac{\mu_{21}}{\mu_{22}} = (1 - C_2 \bar{V}_2)\left(\frac{\mu_{12}}{\mu_{22}} - \frac{C_2 \bar{V}_2}{y_2} \right) + C_2 \bar{V}_1 \qquad (2.21)$$

Typically, $C_2 \bar{V}_2$ in Eq. 2.21 is small (about 5% or less) compared to one and the magnitude $\gamma \equiv \mu_{12} / \mu_{22}$ (keeping in mind that $y_2 \approx 1$). This implies that it may be neglected within the experimental error (about 5%) in cross-diffusion data. Thus Eq. 2.21 can be approximated by:

$$\frac{\mu_{21}}{\mu_{22}} = \gamma + C_2\bar{V}_1 \tag{2.22}$$

Note that Eq. 2.22 was used to obtain Eq. 2.18.2. If $\gamma = 0$, we no net interactions between macromolecule and cosolute in water. In this reference case, we deduce that

$$\hat{D}_{21} \approx \frac{\mu_{21}}{\mu_{22}} = C_2\bar{V}_1 \tag{2.23}$$

where we have also used Eq. 2.20.

We now remark that $\mu_{21}/\mu_{22} = -(\partial C_2/\partial C_1)_{\mu_2}$ is the cosolute partitioning coefficient introduced in the above section. Thus Eq. 2.8 can be rewritten in the following way:

$$-\left(\frac{\partial C_2}{\partial C_1}\right)_{\mu_2, C_1=0} = \gamma + C_2\bar{V}_1 \tag{2.24}$$

Equation 2.23, which is consistent with Eq. 2.20 and Eq. 2.18.2 provides a thermodynamic link between γ and the cosolute partitioning coefficient. We can therefore link γ to the thermodynamics of equilibrium dialysis. In the following two sections, we are going to use equilibrium dialysis to introduce two models, Excluded-Volume and Ligand-binding models, giving an expression for $\gamma(C_2)$ in the case of repulsive ($\gamma > 0$) and attractive ($\gamma < 0$) interactions, respectively.

2.5.1 Excluded Volume Model

Macromolecule-cosolute net repulsive interactions in water may be described by employing the excluded volume model. To introduce the excluded-volume model, we consider an equilibrium dialysis setup as shown in Fig. 2.1. In this setup, the left compartment contains a ternary macromolecule(1)-cosolute(2)-solvent system with composition specified by the

concentrations (C_1, C_2). This ternary system is separated from a binary cosolute-solvent reservoir (right compartment), with composition specified by the cosolute concentration C_2', by a membrane not permeable to the macromolecules. At equilibrium, the chemical potential of the cosolute, μ_2, must be the same in both compartments. However, due to macromolecule-cosolute interactions, C_2 in the left compartment will be generally different from C_2' in the right compartment.

As a starting point, we can consider the case in which no macromolecule is present inside the left compartment. This implies that $C_1 = 0$ and $C_2 = C_2'$. Upon the insertion of macromolecules, cosolute molecules will diffuse from the left compartment to the right compartment in the presence of repulsive interactions. This implies that C_2 becomes smaller than C_2'. It is important to note that C_2' in the right compartment remains the same since the binary reservoir is set to be infinitely large. Thus, the value of the cosolute chemical potential $\mu_2(C_2')$ in the right compartment will also remain constant. If the two compartments are in chemical equilibrium with respect to the cosolute, the cosolute chemical potential in the right compartment will be always equal to $\mu_2(C_2')$ independent of C_1.

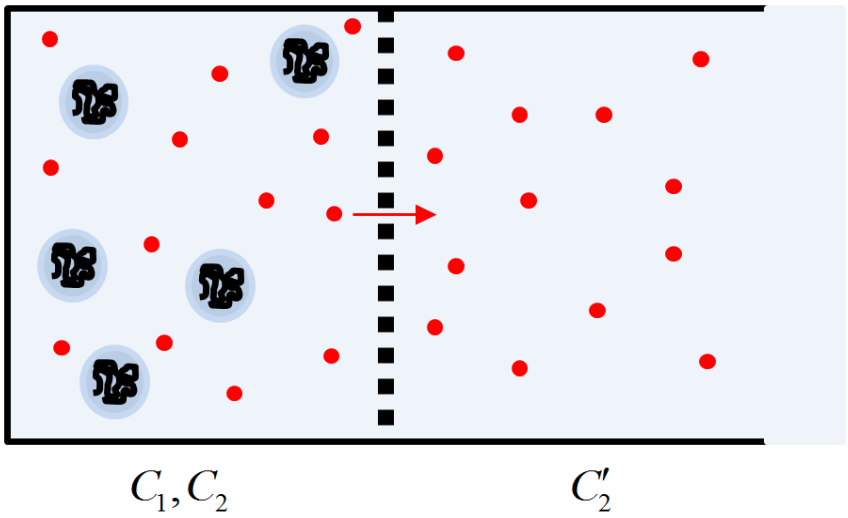

Figure 2.1: The effect of excluded volume on an equilibrium dialysis model separated by a membrane (dashed line) permeable to cosolute and water molecules only and not polymer molecules. The left compartment contains polymer (coils) with cosolute (small red spheres) and water (light blue background). The space surrounding each coil (dark blue circles) describes the volume excluded to the cosolute. The right compartment contains only cosolute particles and water in an open large binary reservoir. The red arrow describes the net transport of cosolute from the left to the right compartment due to polymer-cosolute repulsive interactions.

To describe the difference between C_2 and C_2', it is convenient to introduce the cosolute partitioning coefficient:

$$\left(\frac{\partial C_2}{\partial C_1}\right)_{\mu_2, C_1=0} = \left(\frac{\partial C_2}{\partial C_1}\right)_{C_2', C_1=0} = \lim_{C_1 \to 0} \frac{C_2 - C_2'}{C_1} \tag{2.25}$$

where the subscripts, μ_2 and C_2', specify that these quantities remain constant when C_1 is varied. The quantity $\left(\partial C_2 / \partial C_1\right)_{\mu_2} \equiv \left(\partial C_2 / \partial C_1\right)_{C_2'}$ can be interpreted using the excluded volume model. In this model, we assume that the insertion of one mole of macromolecules introduces a domain surrounding the macromolecule (local domain) that is excluded to the cosolute molecules. The molar volume of the local domain is denoted as V_{ex}. This local domain can be thought as a second dispersed microphase depleted in cosolute within the volume occupied by the ternary system. The volume fraction of this microphase (local domain) is equal to

$(V_{ex}n_1)/V = V_{ex}C_1$, where n_1 and V are the number of macromolecule moles and ternary compartment volume, respectively. The remaining volume of the ternary system (bulk volume) is assumed to remain unperturbed in the presence of macromolecules. Thus, the cosolute concentration in the bulk domain must be equal to C_2'. The overall cosolute concentration in the ternary system, C_2, will be the volume-weighted average of the cosolute concentrations in the local and bulk domain; i.e., $C_2 = (C_1V_{ex})\cdot 0 + (1-C_1V_{ex})\cdot C_2'$. This implies that

$$C_2 = (1-C_1V_{ex})\cdot C_2' \tag{2.26}$$

We are now in position to use Eq. 2.26 to take the partial derivative $(\partial C_2/\partial C_1)_{C_2'}$. We therefore obtain:

$$\left(\frac{\partial C_2}{\partial C_1}\right)_{\mu_2, C_1=0} = \left(\frac{\partial C_2}{\partial C_1}\right)_{C_2', C_1=0} = -V_{ex}C_2 \tag{2.27}$$

where we have also used $C_2 = C_2'$ when $C_1 = 0$. The excluded volume term, V_{ex}, can be described as the summation of the volume occupied by the dry macromolecule and that of the surrounding solvent (0). We can write:

$$V_{ex} = \bar{V}_1 + N_w\bar{V}_0 \tag{2.28}$$

where $\bar{V}_1$ and $\bar{V}_0$ are the molar volumes of the macromolecule and solvent, respectively. The term, N_w, corresponds to the number of solvent molecules in the local domain according to the outlined excluded-volume model. It is important to remark that this model assumes that the concentration of cosolute is *zero* inside the local domain. In general, this need not be the case because repulsive interactions only imply that the cosolute concentration in the local domain is *lower* than that inside the bulk domain, not necessarily zero. Thus, the term N_w should be more

generally interpret as *excess* of solvent molecules in the local domain. We therefore denote N_w as the excess of solvent molecules surrounding the macromolecule. It is also important to remark that this excluded-volume model makes no inference on whether this water is actually bound to the macromolecule.

Within the framework of the Kirkwood-Buff theory of ternary liquid solutions, N_w is linked to the radial function describing the local cosolute concentration as a function of the distance from the center of the macromolecule.[34] This generalization is important for appreciating that negative values of N_w, which cannot be described in the simple excluded volume model, imply a depletion of solvent in the local domain and a corresponding enrichment of cosolute. This latter case is typically interpreted as an actual binding of the cosolute to the macromolecule. In the following section, a binding model is reported to describe the case of macromolecule-cosolute net attractive interactions. In conclusion, according to Eqs. 2.28 and 2.22, the expression of the thermodynamic parameter γ is[11]

$$\gamma = N_w \bar{V}_0 C_2 \tag{2.29}$$

2.6 Ligand Binding Model

To introduce the ligand-binding model, we consider the same equilibrium dialysis setup used for the excluded-volume model in Fig. 2.1. At equilibrium, the chemical potential of the cosolute, μ_2, must be the same in both compartments. In this model, the cosolute is assumed to bind to the macromolecules as shown in Fig. 2.2. The cosolute concentration in the binary reservoir, C_2', is assumed to be equal to the unbound cosolute concentration in the available volume of the ternary compartment. In this model, Eq. 2.26 is replaced by

$$C_2 = (1 - C_1 \bar{V}_1) \cdot C_2' + \nu_L C_1 \tag{2.30}$$

where ν_L is the number of bound cosolute molecules per polymer coil. In this equation, the total cosolute concentration in the ternary compartment is the summation of two terms. The $\nu_L C_1$ term represents the concentration of the total bound cosolute while $(1-C_1\bar{V}_1)\cdot C_2'$ is the concentration of free solute in the total volume of the ternary compartment, where the factor $(1-C_1\bar{V}_1)$ accounts for a residual excluded-volume contribution related to the macromolecule steric contribution. Note that ν_L is a function of C_2' independent of C_1. Specifically, ν_L increases as C_2' increases starting from $\nu_L = 0$ at $C_2' = 0$.

As in the previous section, we use Eq. 2.30 to take the partial derivative $\left(\partial C_2 / \partial C_1\right)_{C_2'}$. We therefore obtain:

$$\left(\frac{\partial C_2}{\partial C_1}\right)_{\mu_2, C_1=0} = \left(\frac{\partial C_2}{\partial C_1}\right)_{C_2', C_1=0} = -C_2\bar{V}_1 + \nu_L \tag{2.31}$$

Note that $\nu_L(C_2') = \nu_L(C_2)$ in the limit of $C_1 \to 0$. Using Eq. 2.31, we finally obtain:

$$\gamma = -\nu_L \tag{2.32}$$

This expression for the ligand-binding model can be also used to link ν_L to N_w. Comparison of Eq. 2.29 with Eqs. 2.31 and 2.32 allows us to deduce that

$$N_w = -\frac{\nu_L}{\bar{V}_0 C_2} \tag{2.33}$$

which shows that N_w is negative in the presence of cosolute binding as expected. To further examine the behavior of ν_L we can use the Scatchard binding model. This model assumes that a

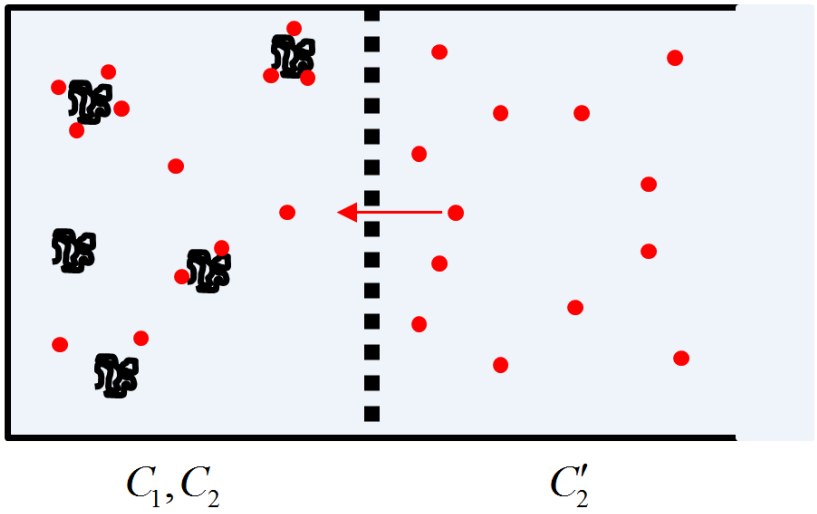

Figure 2.2: The effect of the ligand binding molecule in an equilibrium dialysis model separated by a membrane (dashed line) permeable to cosolute and water molecules only and not polymer molecules. . The left compartment contains polymer (coils) with cosolute (small red spheres) and water (light blue background). The right compartment contains only cosolute particles and water in an open large binary reservoir. The red arrow describes the net transport of cosolute from the right to the left compartment due to polymer-cosolute attractive interactions.

macromolecule has a finite number of equivalent independent sites. In the limit of $C_1 \to 0$, we have

$$\nu_L = \frac{n(C_2/K)}{1+(C_2/K)} \tag{2.34}$$

where n is the total number of sites on the macromolecule and K is the dissociation constant of a cosolute molecule from the macromolecule. Correspondingly, the value of N_w is $-n/(\bar{V}_0 K)$ at $C_2 = 0$ and its magnitude decreases as C_2 increases. A generalization of the Scatchard model is given by the Hill model:

$$\nu_L = \frac{n(C_2/K)^{n_H}}{1+(C_2/K)^{n_H}} \tag{2.35}$$

Where n_H is the Hill coefficient, with $n_H = 1$ (non-cooperativity) for the Scatchard model. The cases of $0 < n_H < 1$ and $1 < n_H < n$ describe binding anti-cooperativity and cooperativity, respectively.

2.7 Examination of the transport parameter, λ

The transport parameter λ is related to the transport coefficients, L_{12} and L_{11}. In the limit of $C_1 \to 0$, we know that $RTL_{11}/C_1 = D_1^0$ represents the Brownian mobility of the macromolecule (see Eq. 2.11). However, to understand λ, we also need to examine what L_{12} represents. In this section, the physical interpretation of the Onsager transport coefficients, L_{ij} 's, is discussed by introducing a friction formalism. We start by considering a binary solute(1)-solvent(0) system and then extend our discussion to ternary macromolecule(1)-cosolute(2)-solvent(0) system.

A diffusion process can be thought to occur in a quasi-stationary regime in which the diffusion driving forces, $-\nabla\mu_1$, equal the opposing frictional force due to the difference in net migration rates, r_i, between the solute(i=1) and the solvent(i =0):

$$-\nabla\mu_1 = C_0 \, f_{10}(r_1 - r_0) \tag{2.36}$$

where f_{10} is a coefficient describing the frictional force between solute molecule 1 and solvent molecule 0. The solvent concentration, C_0 in Eq. 2.36, takes into account the total interaction of one solute molecule with all molecules of solvent per unit of volume. Eq. 2.36 can be used to derive an expression for L_{11}:

$$L_{11} = \frac{C_1}{C_0 f_{10}} \tag{2.37}$$

We now extend this frictional formalism to ternary macromolecule(1)-cosolute(2)-solvent(0) system in the following way:

$$-\nabla\mu_1 = C_0 f_{10}(r_1 - r_0) + C_2 f_{12}(r_1 - r_2) \tag{2.38}$$

$$-\nabla\mu_2 = C_1 f_{21}(r_2 - r_1) + C_0 f_{20}(r_2 - r_0) \tag{2.39}$$

where f_{10} and f_{20} describe the friction of macromolecule(1) and cosolute(2) with water, respectively.[4] The frictional coefficient, $f_{12} = f_{21}$, characterizes the friction due to the difference in net migration rates, r_i, between the macromolecule (i=1) and cosolute (i =2). According to the microscopic physical interpretation of friction, the f_{ij} 's are expected to be positive quantities.

In the matrix form, Eqs. 2.38, 2.39 become:

$$-\begin{bmatrix} \nabla\mu_1 \\ \nabla\mu_2 \end{bmatrix} = \begin{bmatrix} \dfrac{C_0 f_{10} + C_2 f_{12}}{C_1} & -f_{12} \\ -f_{21} & \dfrac{C_0 f_{20} + C_1 f_{21}}{C_2} \end{bmatrix} \begin{bmatrix} J_1 \\ J_2 \end{bmatrix} \tag{2.40}$$

Comparison with Eq. 2.19 leads to

$$\begin{bmatrix} L_{11} & L_{12} \\ L_{21} & L_{22} \end{bmatrix} = \begin{bmatrix} \dfrac{C_0 f_{10} + C_2 f_{12}}{C_1} & -f_{12} \\ -f_{21} & \dfrac{C_0 f_{20} + C_1 f_{21}}{C_2} \end{bmatrix}^{-1} = \det(L) \begin{bmatrix} \dfrac{C_0 f_{20} + C_1 f_{21}}{C_2} & f_{12} \\ f_{21} & \dfrac{C_0 f_{10} + C_2 f_{12}}{C_1} \end{bmatrix} \tag{2.41}$$

Note that $L_{12} = f_{12}\det(L)$ and the ORR corresponds to $f_{12} = f_{21}$. Since $\det(L)$ is a positive quantity, the sign of L_{12} is the same as that of f_{12}. Thus, according to the microscopic physical interpretation of friction, L_{12} is expected to be positive quantity. In the limit of $C_1 \to 0$, we finally obtain:

$$\lambda = -\frac{f_{12}}{f_{20}}\frac{C_2}{C_0} \tag{2.42}$$

According friction formalism, λ is expected to be a negative quantity. However recent experimental results have shown that λ is a positive quantity for PEG in the presence of salting-out salts. This goes against the friction interpretation. In the following section, we are going to to introduce a model, hydration model, showing why $\lambda(C_2)$ can be a positive quantity.

2.8 Hydration model

To overcome the paradox of negative friction coefficients, the net hydrophilic nature of macromolecules in the presence of salting-out salts and osmolytes needs to be considered. These macromolecules may diffuse together with *bound* water molecules due to preferential hydration. In other words, the actual diffusing particle is a hydrated macromolecule not a dry macromolecule. We therefore assume that a hydrated macromolecule is formed according to

$$\mathrm{P} + n_w \mathrm{H_2O} \to \mathrm{P(H_2O)}_{n_w}$$

where n_w is the number of water molecules travelling with the macromolecule. Note that n_w is a positively defined quantity describing the number of water molecules actually bound to the

macromolecule. This can be regarded as a fraction of N_w, previously introduced in Section 2.5.1.[1] The corresponding gradient of the hydrated macromolecule is given by

$$\nabla\mu_1' = \nabla\mu_1 + n_{\mathrm{w}}\nabla\mu_0 = \left(1 - n_{\mathrm{w}}\frac{C_1}{C_0}\right)\nabla\mu_1 - n_{\mathrm{w}}\frac{C_2}{C_0}\nabla\mu_2 \tag{2.43}$$

where μ_1' is the chemical potential of the hydrated macromolecule and we have used the Gibbs-Duhem equation: $C_1\nabla\mu_1 + C_2\nabla\mu_2 + C_0\nabla\mu_0 = 0$. Since the flux of the solvent is zero (solvent-fixed reference frame, ($J_0 = 0$), the flux of *free* water is given by

$$J_0' = -n_w J_1 \tag{2.44}$$

where C_0' and J_0' are the concentration and flux of free solvent, respectively. We now apply the frictional formalism by replacing the dry macromolecule and the total solvent with the hydrated macromolecule and the free solvent, respectively. We have:

$$-\nabla\mu_1' = C_0' f_{10}(r_1 - r_0') + C_2 f_{12}(r_1 - r_2) \tag{2.45}$$

$$-\nabla\mu_2 = C_1 f_{21}(r_2 - r_1) + C_0' f_{20}(r_2 - r_0') \tag{2.46}$$

where r_0' is the migration rate of free solvent. From Eqs. 2.43-2.46, it can be then shown that Eq. 2.39 is replaced by:[49]

$$-\begin{bmatrix} 1 - n_{\mathrm{w}}\dfrac{C_1}{C_0} & -n_{\mathrm{w}}\dfrac{C_2}{C_0} \\ 0 & 1 \end{bmatrix}\begin{bmatrix} \nabla\mu_1 \\ \nabla\mu_2 \end{bmatrix} = \begin{bmatrix} \dfrac{C_0 f_{10} + C_2 f_{12}}{C_1} & -f_{12} \\ -(f_{21} - n_w f_{20}) & \dfrac{C_0\left(1 - n_{\mathrm{w}}\dfrac{C_1}{C_0}\right) f_{20} + C_1 f_{21}}{C_2} \end{bmatrix}\begin{bmatrix} J_1 \\ J_2 \end{bmatrix} \tag{2.47}$$

We can then obtain the following expression for the L_{ij} 's:

$$\begin{bmatrix} L_{11} & L_{12} \\ L_{21} & L_{22} \end{bmatrix} = \begin{bmatrix} \dfrac{C_0 f_{10} + C_2 f_{12}}{C_1} & -f_{12} \\ -(f_{21} - n_w f_{20}) & \dfrac{C_0\left(1 - n_w \dfrac{C_1}{C_0}\right) f_{20} + C_1 f_{21}}{C_2} \end{bmatrix}^{-1} \begin{bmatrix} 1 - n_w \dfrac{C_1}{C_0} & -n_w \dfrac{C_2}{C_0} \\ 0 & 1 \end{bmatrix} \tag{2.48}$$

In the limit of $C_1 \to 0$, Eq. 2.48 yields:

$$\lambda = \left(n_w - \frac{f_{12}}{f_{20}} \right) \frac{C_2}{C_0} \tag{2.49}$$

In the presence of highly hydrophilic macromolecules, we may neglect the friction term in λ, and a good approximation is given by:[1]

$$\lambda = n_w \bar{V}_0 C_2 \tag{2.50}$$

where n_w is solvent molecules bound to macromolecule and we have used $\bar{V}_0 = 1/C_0$ (with $C_2 \bar{V}_2 << 1$). When we insert Eqs. 2.50 and 2.29 into 2.18.1 then $\hat{D}_{12}$ is:

$$\hat{D}_{12} = (N_w - n_w) \bar{V}_0 C_2 \tag{2.51}$$

Note that $\hat{D}_{12}$ is a positive quantity directly proportional to the difference between N_w (with $N_w > 0$) and n_w (with $n_w / N_w < 1$).

Chapter 3

Materials and Methods

3.1 Materials

Poly(ethylene glycol) with an average molecular weight of $20\,\mathrm{kg\cdot mol^{-1}}$ (purity, 99%) was purchased from Sigma Aldrich. For PEG, certificates of analysis obtained from Sigma-Aldrich give the number (Mn) and mass average (Mw) molecular weights based on size exclusion chromatography: Mn =18.00 $\mathrm{kg\cdot mol^{-1}}$ and Mw/Mn =1.37. Urea (ACS certified) was purchased from Fisher Scientific (purity, 99.7%; molecular weight $60.06\,\mathrm{g\cdot mol^{-1}}$). Trimethylamine N-oxide dehydrate (TMAO) was purchased from Acros Organics (purity, 98%; molecular weight (dry) $75.11\,\mathrm{g\cdot mol^{-1}}$, (dihydrate) $111.14\,\mathrm{g\cdot mol^{-1}}$). All chemicals were used without further purification.

3.2 Preparation of stock solutions, binary PEG-water, and TMAO-water

Stock concentrated solutions of PEG and TMAO were made by weight to 0.1 mg. Density measurements (Mettler-Paar DMA40 density meter) were performed on the stock solutions for buoyancy corrections. Stock solutions of TMAO were filtered using Thermo Scientific 90 mm, 500 ml filter. Deionized water was passed through a four-stage Millipore filter system to provide high-purity water for all the experiments. All solutions were prepared by mass. Solid urea was used and measured by mass to the nearest 0.1 mg.

The TMAO weight fraction of the stock solution was determined by measuring its density and using the available density-weight fraction relation at 298.15 K. [49] A plot of density values, d, as a function of TMAO weight fraction, w, was made (see Fig. 3.1) and a best fit

third-degree polynomial expression, $d = d_0(1 + Aw + Bw^2 + Cw^3)$, was determined with $d_0 = 0.99703946\,\mathrm{g \cdot cm^{-3}}$, $A = 0.01862050$, $B = 0.04096804$ and $C = 0.08087050$. This equation was used to determine the weight fraction of the binary TMAO-water stock solutions, w, from the measured density.

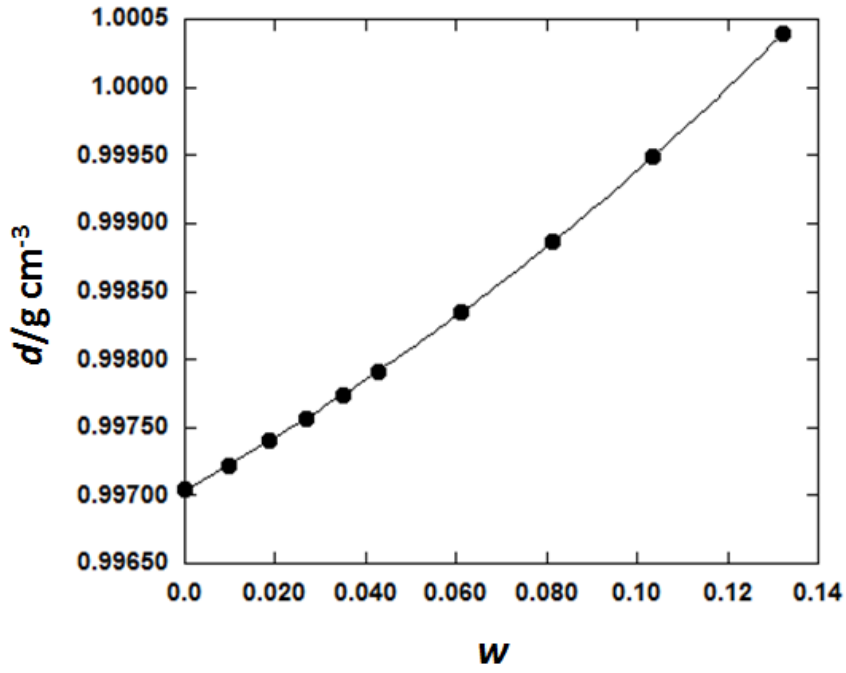

Figure 3.1: Density of the binary TMAO-Water system at 25ºC as a function of TMAO weight fraction, *w*.

3.2.1 Binary PEG-Water, TMAO-water, and Urea-Water Solutions

For binary PEG−water experiments, PEG stock solutions were diluted with pure water to reach the target PEG concentrations. In the binary TMAO−water experiments, TMAO stock solutions were diluted with pure water to reach the target TMAO concentrations. Finally, in the binary urea−water solutions, pure solid urea was added to flasks and diluted with pure water to reach the target urea concentrations.

3.2.2 Preparation of Ternary Solutions

For ternary PEG-cosolute-water solutions, PEG stock solution and cosolute (pure or stock solution) were added to flasks and diluted with pure water to reach the target PEG and cosolute concentrations. Solution densities were measured to determine partial molar volumes and molar concentrations of polymer (C_1, based on the molecular weight of $20\,\mathrm{kg\cdot mol^{-1}}$) and cosolute ($C_2$).

3.3 Rayleigh Interferometry

Binary and ternary mutual diffusion coefficients were measured at 25.00 ± 0.01 °C with the Gosting Diffusiometer operating in the Rayleigh interferometric optical mode.[21] The refractive-index profile inside a diffusion cell is measured as described in ref 4 and references therein. This yields diffusion coefficients in the volume-fixed reference frame.[39,40] The ternary diffusion coefficients, $(D_{ij})_{\mathrm{V}}$, were obtained by applying the method of the nonlinear least-squares to the refractive-index profiles.[45,66] Due to PEG molecular-weight polydispersity, a corrective procedure in ref 46 and 67 based on the experimental refractive-index profiles of binary PEG−water systems was applied to our ternary experiments in order to remove the contribution of polydispersity from the ternary refractive-index profiles**.** The precision of the diffusion coefficient values was estimated to be equal to about 0.1% in the case of binary systems.[46-51]

We now review the Rayleigh interferometric method as well as the fundamental equations which are used for the determination of the multicomponent diffusion coefficients. The Rayleigh method yields the one-dimensional profile of the refractive index of a liquid system

contained in a rectangular cell. This one-dimensional refractive index profile, under given initial and boundary conditions, is utilized to obtain diffusion coefficients. Rayleigh interferometry can be used as one of the most accurate methods to obtain refractive index profiles to measure the diffusion coefficient.

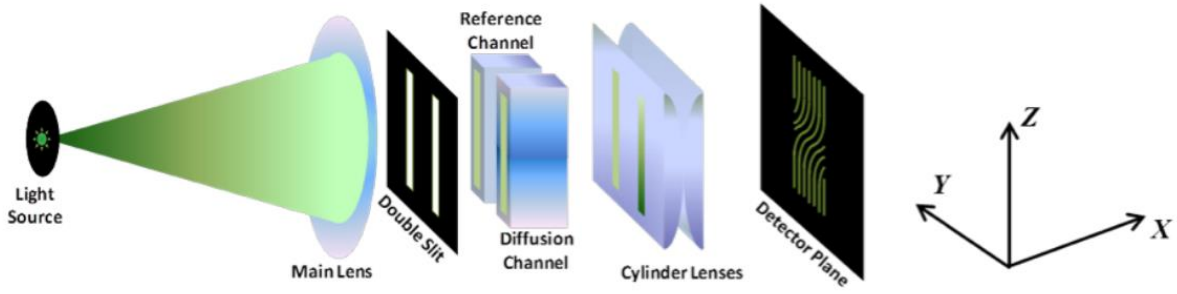

Figure 3.2**:** Optical apparatus operating by Rayleigh interferometry.

The light from a laser source is sent to a main spherical lens, which in turn focuses the beam onto the detector plane (see Figure 3.3). After the beam passes trough the lens, it is split into two parts by two narrow vertical slits positioned between the lens and the cell. One beam goes through the diffusion channel and one through the reference channel. The interference pattern generated by the superposition of the two beams is recorded on the detector plane. The distance between the fringes is determined by the separation of the two slits, while the absolute shift of the fringes is proportional to the difference in the optical path between the two beams. If the refractive index is uniform in the diffusion channel along the Z-direction (see Figure 3.2), the value of the position Y of the maxima at the detector plane is independent of Z. Thus straight interference vertical lines are produced. If the refractive index inside the diffusion channel changes along the Z-direction, the position of the maxima will shift along the same direction of a quantity proportional to the shift in the refractive index. This generates the interference pattern shown in

Fig. 3.2. Since the rays are deflected by the gradient of refractive index, a system of cylinder lenses is needed to effectively reverse the deflection and focus the cell to the detector "plane".

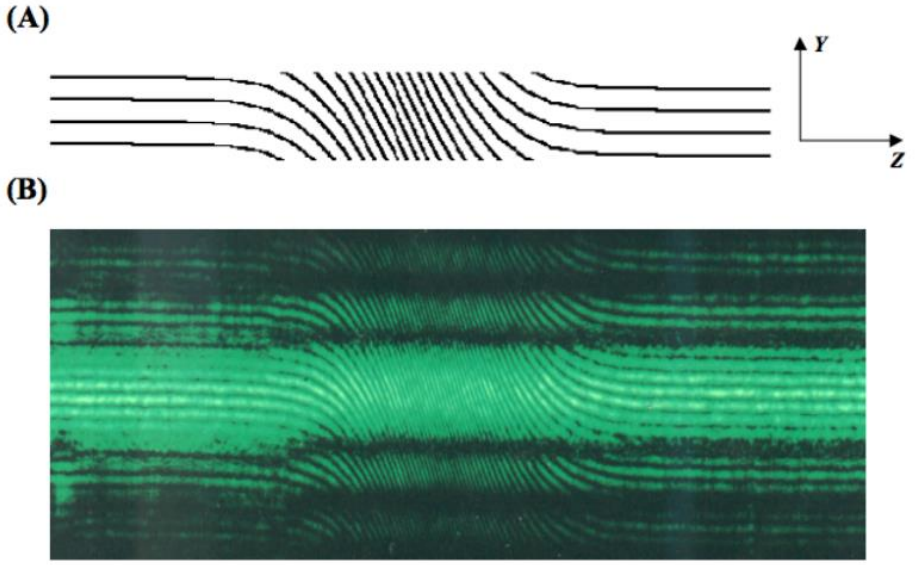

Figure 3.3 (Fringes): (A) Scheme of the Rayleigh interferometric pattern; the solid lines correspond to maxima positions. (B) Picture of the Rayleigh interferometric pattern taken from the Gosting diffusiometer.

The Gosting diffusiometer located at Texas Christian University was used to measure diffusion coefficients based on Rayleigh interferometry. [52-54] A side view of the diffusiometer (optical-bench length of 8.84 m) is shown in Figure 3.4.[13] The light source used is a 0.5 mW Uniphase He-Ne LASER with a wavelength $\lambda = 543.5$ nm (in air). The main lens (focal length of 145.16±0.03 cm) is installed in a lens mount on the source slit side of the water bath so that the diffusion cell is in the converging light between the lens and the detector.[49,43]

The cylinder lens consists of two plane-convex lenses, each 7.5 cm square and 1.3 cm thick at its thickest part. A cell holder is used to locate the cell in the bath and to support a mask located between the cell and the light source. The mask consists of a double window allowing

the beam to split in two parts one going through the diffusion channel and the other passing directly in the water bath (reference channel). The cell is a glass.

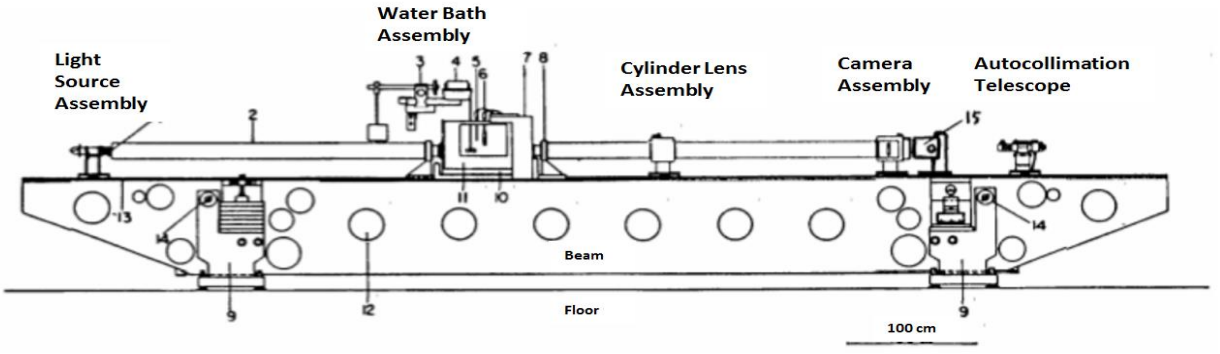

Figure 3.4: Schematic drawing of the diffusiometer. Components in the diagram are as follows: 1. light source, 2. tube to minimize air current in the light path, 3. stirring motor mount, 4. sensor of temperature control, 5. heater, 6. cell frame support, 7. special window rider, 8. beam support, 9. water bath support, 10. access hole to reach inside the beam, 11. ways, 12. leveling collar to check any change in the position of the beam relative to the beam support, 13. digital optical scanner.

Figure 3.5 shows the main features of the cell. The cell is composed of three pieces put in contact by very smooth planes surfaces. Grease is used to seal the plates and lubricate sliding relative to each other. The shift of the plates allows the solutions, filled in all three parts, to be either in contact or isolated from each other. The right side of the middle part contains the solution to be optically investigated (diffusion channel). The reference channel is located on the right side of the diffusion channel. The path length for the cell (model C-1235-H11) employed in the measurements is l = 2.505 cm. Data is recorded from Rayleigh interference patterns using a vertical linear photodiode array (6 cm long, 6000 pixel, (10x10 μm pixels) linear photodiode array model IL-C8-6000-64 with good light sensitivity) that moves horizontally through the pattern through the use of a stepping motor and a processing screen. All programming of scanner controls and data analysis was done in Borland C++ for DOS.

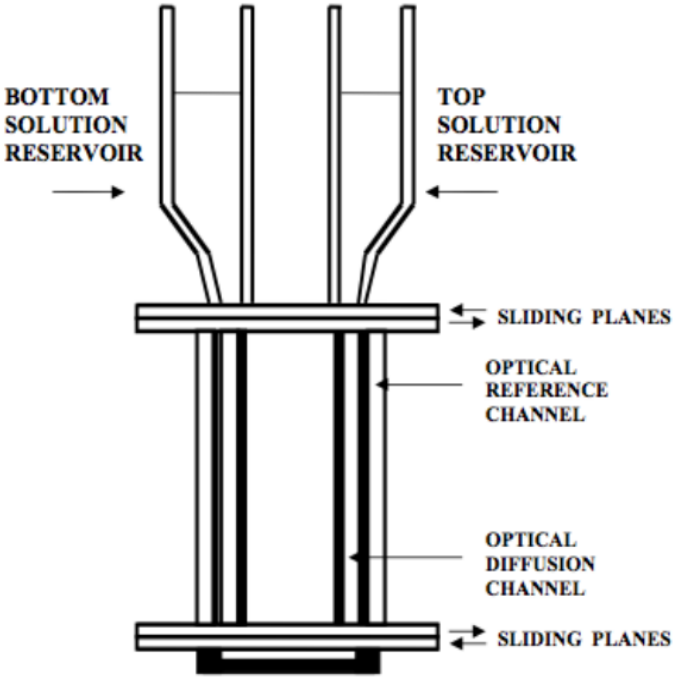

Figure 3.5 Cell

The most important step for a successful experiment is the preparation of a good initial condition from which the diffusion process will be investigated in its evolution. The two solutions with different compositions in the diffusion channel are in contact. The denser solution is located at the bottom part of the diffusion channel (a necessary condition for avoiding convection). The top solution interfaces with the bottom solution. A flat and sharp intermediate boundary is obtained by lowering a needle to the optic axis of the diffusion channel. The solutions are drawn out of the cell through the needle with a peristaltic pump. When sufficient time has elapsed after the needle is removed, diffusion patterns clearly emerge which can be resolved by the optical scanner. Diffusion scans (usually 50), equally distributed in the testing time frame, are performed. The refractive index profile along the vertical Z direction is then extracted. However, the projection of the cell onto the detector plane is magnified. Thus a magnification factor is needed to convert the positions on the Z-axis of the image into the

corresponding positions inside the cell. The magnification factor can be easily evaluated by projecting a grating scale located in the cell holder onto the detector plane. The interference demonstrates a gradient of refractive index which is directly proportional to the number of fringes.

The refractive index change as a function of time and position is conveniently defined by the normalized function: $f(j) \equiv (2j - J)/J$ where j is a continuous variable with values ranging between 0 and the total number of fringes J. This function has the property to be zero at the center of the pattern and equal to respectively -1 and +1 at the boundaries. Well-established time-correction and anti-symmetrization procedures (Creeth-pair method) are applied to $f(j)$ in order to remove boundary imperfections, lens aberration and concentration-dependence of diffusion coefficients.[48,49,43]

3.4 Determining the Diffusion coefficients from Rayleigh Interferometry

For a binary system, the diffusion equation[43] can be solved with the free-diffusion boundary condition to obtain :[38]

$$f(j) = \text{erf}\left(\frac{x}{2\sqrt{tD}}\right) \tag{3.1}$$

where x is the position (the vertical distance from the solutions initial boundary and parallel to the Z direction in Figs. 3.1 and 3.2), t is time, D is the diffusion coefficient, and $\text{erf}(y) \equiv (2/\sqrt{\pi})\int_0^y e^{-z^2} dz$. For each x, t and $f(j)$, a value of D is obtained using Equation 3.2. The final value of the diffusion coefficient is calculated by taking the average of all D values.[38,43] For a ternary system, one can solve the diffusion equation with the free-diffusion boundary condition and obtain:

$$f(j) = \Gamma_1 \mathrm{erf}\left(\frac{x}{2\sqrt{t\Lambda_1}}\right) + \Gamma_2 \mathrm{erf}\left(\frac{x}{2\sqrt{t\Lambda_2}}\right) \tag{3.2}$$

where Λ_1 and Λ_1 are the eigenvalues of the matrix of four diffusion coefficients. In Equation 3.3 and 3.4, $\alpha_i = R_i \Delta C_i / \Delta n$ and $R_i \equiv (l/\lambda)(\partial n / \partial C_i)_{T,P,C_j,i\neq j}\, \Delta n$ is the difference in refractive index between bottom and top solution, ΔC_i is the difference in molar concentration of component i between bottom and top solution, and a and b are two parameters to be determined.

$$\Gamma_1 = a + b\alpha_1 \tag{3.3}$$

$$\Gamma_2 = 1 - a - b\alpha_1 \tag{3.4}$$

The values of R_1 and R_2 are obtained by applying the method of linear least square to the experimental total number of fringes *J* plotted against (ΔC_1, ΔC_2) using

$$J = R_1 \Delta C_1 + R_2 \Delta C_2 \tag{3.5}$$

The quantity α_1 (or $\alpha_2 = 1 - \alpha_1$) defines the initial condition of an individual experiment. To determine *a* and *b*, at least two experiments at different α_1 need to be performed. Typically four experiments are performed to reduce measurement error. The non-linear least square method is applied to $f(j)$ with respect to the independent variables $x/\sqrt{t}$ and α_1 yielding α_1, α_2, *a* and *b*.

The ternary diffusion coefficients can be then determined by the following set of equations:[39]

$$D_{11} = \frac{\Lambda_1 \Lambda_2}{b}\left[(a+b)(1-a)/\Lambda_2 - a(1-a-b)/\Lambda_1\right] \tag{3.6}$$

$$D_{12} = -\frac{R_2}{R_1}\frac{\Lambda_1 \Lambda_2}{b}(1/\Lambda_1 - 1/\Lambda_2)a(1-a) \tag{3.7}$$

$$D_{21} = \frac{R_1}{R_2}\frac{\Lambda_1\Lambda_2}{b}(1/\Lambda_1 - 1/\Lambda_2)(a+b)(1-a-b) \tag{3.8}$$

$$D_{22} = \frac{\Lambda_1\Lambda_2}{b}[(a+b)/\Lambda_1 - a(1-a-b)/\Lambda_2] \tag{3.9}$$

Finally, a pseudo-binary diffusion coefficient, D_A, can be determined for individual experiments (with a given α_1) on ternary systems. This can be calculated using:

$$\frac{1}{\sqrt{D_A}} = \frac{\Gamma_1}{\sqrt{\Lambda_1}} + \frac{\Gamma_2}{\sqrt{\Lambda_2}} = \frac{a+b\alpha_1}{\sqrt{\Lambda_1}} + \frac{1-a-b\alpha_1}{\sqrt{\Lambda_2}} \tag{3.10}$$

3.5 Density Measurements

Density measurements were taken using a Mettler-Paar DMA40 densitometer with an RS-232 output to a Sony computer. The densitometer has a vibrating tube with temperature controlled by a thermostat attached to a water bath that is 25.00±0.01°C. The solution density *d* is related to the period of vibration of the tube T_v by the following:

$$d = A + BT_v^2 \tag{3.11}$$

where *A*, *B* are two instrumental constants. The determination of these constants is based on two reference periods air ($d_{air} = 0.00115\ \mathrm{g\cdot cm^{-3}}$) and water ($d_{water} = 0.997045\,\mathrm{g\cdot cm^{-3}}$). An accurate value of the density of air was estimated by a state equation that shows dependence on the pressure, temperature (25.00 °C), and humidity.

Density measurements are required for calculation of both molar concentrations and partial molar volumes, $\bar{V}_i \equiv (\partial V/\partial n_i)_{T,P,n_{j,i\neq j}}$ with $i, j = 0,\ 1,\ 2$. For the diffusion experiments, several pairs of solutions with different concentrations were prepared at the same average

composition. This characterization is known as the average composition, ($\bar{C}_1, \bar{C}_2$). Since the compositions of these solutions show relatively small differences with respect to the mean, the concentration dependence for the density is usually assumed to be linear:[46]

$$d(C_1, C_2) = d(\bar{C}_1, \bar{C}_2) + H_1 \cdot (C_1 - \bar{C}_1) + H_2 \cdot (C_2 - \bar{C}_1) \tag{3.12}$$

where the $H_i \equiv (\partial d_i, \partial C_i)_j$. The solute partial molar volumes corresponding to the mean composition, can be then calculated by:[39]

$$\bar{V}_i = \frac{M_i - H_i}{\bar{d} - H_1\bar{C}_1 - H_2\bar{C}_2} \tag{3.13}$$

$i = 1, 2$ and where M_i is the molar weight of the component i. The solvent partial molar volume can be calculated by applying the following condition:

$$\bar{V}_0 C_0 + \bar{V}_1 C_1 + \bar{V}_2 C_2 = 1 \tag{3.14}$$

Chapter 4

Results

4.1 Results

In this chapter, our experimental diffusion coefficients for the binary cosolute(2)-water(0) and PEG(1)-cosolute(2)-water(0) systems are reported at 25°C. All ternary experiments were performed at the low PEG molar concentration of 2.50×10^{-4} mol·dm^{-3}.

4.2 Diffusion coefficients for the binary cosolute(2)-water(0) systems

In table 4.1 and 4.2 our experimental diffusion coefficient results for the binary TMAO(2)-water(0) and urea(2)-water(0) systems are reported. The experimental error on the binary diffusion coefficients is about 0.1%. Other related thermodynamic and transport parameters, which were taken from literature and are needed for calculating $\hat{D}_{12}$ and $\hat{D}_{21}$, are also included.

From tables 4.1 and 4.2, we can see that TMAO and urea have very different viscosity and activity-coefficient properties in water. For example, the relative viscosity, η_r, in the TMAO case is about 34% higher than that measured in the urea case at the cosolute concentration of $1\ \mathrm{mol}\cdot\mathrm{dm}^{-3}$. Furthermore, the thermodynamic factor, y_2 (refer to eq. 2.14), in the TMAO case is 50% higher than that predicted for ideal-dilute solutions at $C_2 = 1\ \mathrm{mol}\cdot\mathrm{dm}^{-3}$. On the other hand, y_2 remains close to one in the urea case at this concentration. This indicates significant net repulsive TMAO-TMAO net interactions in water.

Table 4.1: Thermodynamic and transport properties for the TMAO-water system at 25°C.

C_2 /mol dm^{-3}	$\bar{V}_2$ [a] /cm^{3}mol^{-1}	$\bar{V}_0$ [a] /cm^{3}mol^{-1}	$1-C_2\bar{V}_2$	y_2 [b]	η_r [c]	$(D_2)_V$ [d] /10^{-9} m^{2}s^{-1}	$(D_2)_0$ [d] /10^{-9} m^{2}s^{-1}	α [e]
0.25	73.03	18.07	0.982	1.123	1.086	0.911	0.928	0.0540
0.50	72.78	18.07	0.964	1.254	1.179	0.916	0.951	0.0485
1.00	72.25	18.08	0.928	1.545	1.400	0.930	1.002	0.0388

[a]Values of $\bar{V}_2$ and $\bar{V}_0$ were obtained from Ref. 57.[b]Values of y_2 were obtained from Ref. 56. [c]Values of η_r were obtained from Ref. 58. [d]Values of $(D_2)_V$ were obtained from this work, with $(D_2)_0 = (D_2)_V / (1-C_2\bar{V}_2)$. [e]Values of $\alpha \equiv D_\mathrm{P} / (D_2)_0$ were calculated using the PEG tracer diffusion coefficient in water at 25 ºC, $D_\mathrm{P} / 10^{-9}\,\mathrm{m^2 s^{-1}} = 0.0544$. Value of D_P taken from Ref. 8.

Table 4.2: Thermodynamic and transport properties for the urea-water system at 25°C.

C_2 /mol dm^{-3}	$\bar{V}_2$ [a] /cm^{3}mol^{-1}	$\bar{V}_0$ [a] /cm^{3}mol^{-1}	$1-C_2\bar{V}_2$	y_2 [b]	η_r [c]	$(D_2)_V$ [d] /10^{-9} m^{2}s^{-1}	$(D_2)_0$ [d] /10^{-9} m^{2}s^{-1}	α [e]
0.18	44.29	18.07	0.992	0.993	1.007	1.367	1.378	0.0392
0.38	44.34	18.07	0.983	0.985	1.015	1.351	1.374	0.0390
0.80	44.46	18.07	0.964	0.974	1.032	1.319	1.368	0.0385
1.00	44.51	18.07	0.955	0.969	1.041	1.307	1.368	0.0382

[a]Values of $\bar{V}_2$ and $\bar{V}_0$ were obtained from Ref. 60.[b]Values of y_2 were obtained from Ref. 59. [c]Values of η_r were obtained from Ref. 61. [d]Values of $(D_2)_V$ were obtained from this work, with $(D_2)_0 = (D_2)_V / (1-C_2\bar{V}_2)$. [e]Values of $\alpha \equiv D_\mathrm{P} / (D_2)_0$ were calculated using the PEG tracer

We can attribute the fact that y_2 is significantly larger than one for TMAO to the diffusion coefficient in water at 25 ºC, $D_P/10^{-9}\,m^2s^{-1} = 0.0544$. Value of D_P taken from Ref. 8. osmolyte nature of this cosolute. The dependence of the solution osmotic pressure Π on osmolyte concentration, C_2, is given by

$$\left(\frac{\partial \Pi}{\partial C_2}\right)_{T,p} = \frac{RT}{1-C_2\bar{V}_2} y_2 \tag{4.1}$$

with $(\partial\Pi/\partial C_2)_{T,p} = RT$ when $C_2 \to 0$ (ideal-dilute limit). Since $y_2 > 1$, $(\partial\Pi/\partial C_2)_{T,p}$ increases more than expected from $\Pi = RTC_2$. In other words, TMAO significantly increases solution osmotic pressure well above the increase predicted for ideal-dilute solution. Due to the osmotic properties of TMAO, this osmolyte is known to help cells retain water through the cellular membrane. As previously mentioned, cells use TMAO and other osmolytes to maintain volume under conditions of stress (see section on Motivation).

In tables 4.1 and 4.2, we also report the partial molar volumes of cosolute and water. These data allow us to deduce that $1-C_2\bar{V}_2$ ranges from 0.93 to 0.98 within our experimental cosolute concentration ranges. Furthermore, the values of water partial molar volumes are essentially the same as the molar volume of pure water ($18.07\,cm^3\cdot mol^{-1}$).

In tables 4.1 and 4.2, we report both the measured mutual diffusion coefficients in the volume-fixed reference frame $(D_2)_V$ and the corresponding solvent-fixed diffusion coefficients $(D_2)_0$. We can see that the urea diffusion coefficients (≈1.3….) are about 40% higher than the TMAO ones (≈0.9….). For comparison, the partial molar volumes of TMAO are about 60% higher than those of urea. Assuming that partial molar volumes are proportional to the corresponding hydrodynamic volumes, the difference between the diffusion coefficients of

TMAO and urea is in qualitative agreement with the size trend predicted from the Stokes-Einstein equation. The last column in tables 4.1 and 4.2 reports the cosolute-polymer diffusion ratios, α. We can see that $\alpha \approx 0.05$ and $\alpha \approx 0.04$ in the TMAO and urea cases, respectively. We therefore expect that the kinetic term in the cosolute osmotic diffusion is small (see eq. 2.18.2 in Chapter 2).

4.3 Diffusion coefficients for the ternary polymer(1)-cosolute(2)-water(0) systems

In Table 4.3 and 4.4, we report the four experimental ternary diffusion coefficients in the volume-fixed reference frame for the PEG-TMAO-water and PEG-urea-water systems, respectively. All measurements were performed at the PEG concentration of $C_1 = 0.25\,\mathrm{mM}$.

Table 4.3: Ternary diffusion coefficients for the PEG-TMAO-water system at 0.2500 mM PEG, C_2 (TMAO), and water at 25 ºC.

C_2 /mol dm^{-3}	$(D_{11})_V$ /10^{-9} m^2 s^{-1}	$(D_{12})_V$ /10^{-12} m^2 s^{-1}	$(D_{21})_V$ /10^{-9} m^2 s^{-1}	$(D_{22})_V$ /10^{-9} m^2 s^{-1}
0	0.0584±0.0001	-	0	-
0.25	0.0548±0.0001	0.062±0.003	12.0±0.2	0.892±0.002
0.50	0.0514±0.0001	0.058±0.002	23.6±0.3	0.902±0.002
1.00	0.0444±0.0001	0.058±0.003	42.6±0.1	0.914±0.002

Table 4.4: Ternary diffusion coefficients for the PEG-urea-water system at 0.2500 mM PEG, C_2 (urea), and water at 25 ºC.

C_2 /mol dm^{-3}	$(D_{11})_V$ /10^{-9} m^2 s^{-1}	$(D_{12})_V$ /10^{-12} m^2 s^{-1}	$(D_{21})_V$ /10^{-9} m^2 s^{-1}	$(D_{22})_V$ /10^{-9} m^2 s^{-1}
0	0.0584±0.0001	-	0	-
0.38	0.0574±0.0001	0.005±0.002	2.5±0.2	1.328±0.001
0.80	0.0564±0.0001	-0.004±0.002	7.4±0.2	1.299±0.001
1.00	0.0558±0.0001	-0.002±0.002	9.3±0.4	1.285±0.002

Table 4.5: Normalized main diffusion coefficients for the PEG-TMAO-water system.

C_2 / mol dm^{-3}	$[(D_{11})_V / (D_1)_V]\eta_r$	$(D_{22})_V / (D_2)_V$
0	1.000	-
0.25	1.019	0.979
0.50	1.038	0.985
1.00	1.064	0.983

Table 4.6: Normalized main diffusion coefficients for the PEG-urea-water system.

C_2 / mol dm^{-3}	$[(D_{11})_V / (D_1)_V]\eta_r$	$(D_{22})_V / (D_2)_V$
0	1.000	-
0.18	0.997	0.985
0.38	0.997	0.983
0.80	0.997	0.985
1.00	0.995	0.983

Since the cross-diffusion coefficients will be examined in the following section, here we will focus on the examination of the two main diffusion coefficients, $(D_{11})_V$ and $(D_{22})_V$. To examine the dependence of $(D_{11})_V$ as a function of cosolute concentration, it is convenient to normalize this diffusion coefficient with respect to its value in water ($C_2 = 0$) and the relative viscosity of the binary cosolute-water solutions (see η_r data in Tables 4.1 and 4.2), consistent with the Stokes-Einstein equation. In Tables 4.5 and 4.6, we report the values of $[(D_{11})_V / (D_1)_V]\eta_r$ calculated from the corresponding data in Tables 4.3 and 4.4 for the PEG-TMAO-water and PEG-urea-water systems, respectively. In Fig. 4.1, these data are plotted as a function of C_2. Here, we can see a significant difference between the TMAO and urea cases. As we increase the concentration of urea, the change of viscosity-corrected polymer diffusivity is relatively small (less than 1%). On the other hand, $[(D_{11})_V / (D_1)_V]\eta_r$ increases significantly with TMAO

concentration. This behavior correlates with that previously observed for PEG in the presence of sodium sulfate, a strong salting-out agent.[1] In Tables 4.5, 4.6, we include the values of $(D_{22})_V / (D_2)_V$, describing co-solute diffusivity. Here, we can see that the ternary values, $(D_{22})_V$, are about 2% lower than the corresponding binary values, $(D_2)_V$. This small difference can be explained by considering a small obstruction effect of the polymer chains on the mobility of the cosolute molecules. In all cases, the effect of PEG on cosolute diffusion in water is small at $C_1 = 0.25\,\text{mM}$.

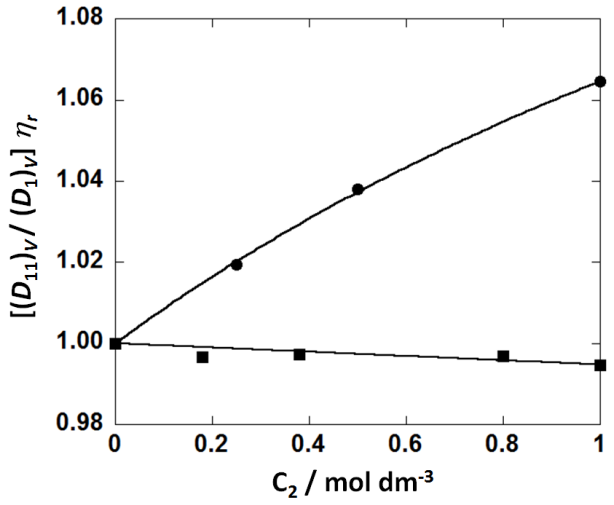

Figure 4.1: Normalized PEG diffusion coefficient as a function of cosolute (TMAO or urea) concentration, C_2 for the PEG-TMAO-water (circles) and PEG-urea-water (squares) systems.

4.3.1 Polymer diffusiophoresis and cosolute osmotic diffusion

In this section, we will discuss the behavior of the cross diffusion coefficients as a function of cosolute concentration. As discussed in Chapter 2, it is convenient to rearrange the cross-diffusion data in Tables 4.3 and 4.4 as $\hat{D}_{12}$ (polymer diffuseophoresis) and $\hat{D}_{21}$ (cosolute osmotic diffusion).

At our low PEG concentration the determined values of $(D_{21})_V/(D_{22})_V$ and $(D_{12})_V/C_1$ are the same as those at $C_1 \to 0$ within the experimental error. This assumption is justified by previous work.[4,5] Note that we consider $(D_{12})_V/C_1$ instead of $(D_{12})_V$, because this cross-diffusion coefficient vanishes in the limit of $C_1 \to 0$. To link our experimental data with $\hat{D}_{12}$ and $\hat{D}_{21}$, we therefore make the following good approximation:

$$\lim_{C_1 \to 0} \frac{(D_{21})_V}{(D_{22})_V} = \frac{(D_{21})_V}{(D_{22})_V} \tag{4.2}$$

$$\lim_{C_1 \to 0} \frac{(D_{12})_V}{C_1} = \frac{(D_{12})_V}{C_1} \tag{4.3}$$

The left sides of Eqs. 4.2 and 4.3 are calculated from the experimental cross-diffusion data in Tables 4.3 and 4.4. The reduced cross-diffusion coefficients are defined with respect to the solvent-fixed reference frame. In the limit of $C_1 \to 0$, Eqs. 2.13.1-2.13.4 can be used to show that

$$\lim_{C_1 \to 0} \frac{(D_{21})_0}{(D_{22})_0} = \lim_{C_1 \to 0} \frac{(D_{21})_V}{(D_{22})_V} + \frac{\alpha C_2 \bar{V}_1}{1 - C_2 \bar{V}_2} \tag{4.4}$$

$$\lim_{C_1 \to 0} \frac{(D_{12})_0}{C_1} = \lim_{C_1 \to 0} \frac{(D_{12})_V}{C_1} + \bar{V}_2 (D_2)_0 \tag{4.5}$$

The second term on the right side of Eqs. 4.4 and 4.5 is calculated from the data on the binary cosolute-water systems in Tables 4.1 and 4.2, and the known partial molar volume of PEG, $\bar{V}_1 = 16.7\,\mathrm{cm^3 mol^{-1}}$. After applying Eqs. 4.4 and 4.5, we are in position to determine $\hat{D}_{12}$ and $\hat{D}_{21}$ from Eqs. 2.14.1, 2.14.2 in Chapter 2. The calculated values of $\hat{D}_{12}$ and $\hat{D}_{21}$ are reported in Tables 4.7 and 4.8.

Table 4.7: Reduced values of $\hat{D}_{12}$ and $\hat{D}_{21}$ for the PEG-TMAO-water system.

C_2 / mol dm^{-3}	$\hat{D}_{12}$	$\hat{D}_{21}$
0	0	0
0.25	1.40±0.05	13.7±0.2
0.50	2.60±0.07	26.6±0.3
1.00	5.07±0.20	47.3±0.1

Table 4.8: Reduced values of $\hat{D}_{12}$ and $\hat{D}_{21}$ for the PEG-urea-water system.

C_2 / mol dm^{-3}	$\hat{D}_{12}$	$\hat{D}_{21}$
0	0	0
0.18	0.27±0.03	1.1±0.2
0.38	0.58±0.06	2.1±0.2
0.80	0.70±0.12	6.2±0.2
1.00	1.04±0.16	8.7±0.2

In Fig. 4.2, the polymer diffusiophoresis parameter, $\hat{D}_{12}$, is plotted as a function of C_2 for the two cosolute cases. In this figure, we can see that the $\hat{D}_{12}$ linearly increases with cosolute concentration starting from $\hat{D}_{12} = 0$ at $C_2 = 0$ in both cases. This implies that a cosolute concentration gradient induces PEG diffusion from high to low cosolute concentration. However, the values of $\hat{D}_{12}$ obtained in the TMAO case are about five-fold larger than those obtained in the urea case at a given cosolute concentration. This qualitatively correlates with PEG-TMAO net interactions being more repulsive than PEG-urea net interactions in water.

In Fig. 4.3, the cosolute osmotic diffusion parameter, $\hat{D}_{21}$, is plotted as a function of C_2 for the two cosolute cases. In this second figure, we can also see that the $\hat{D}_{12}$ increases with cosolute concentration starting from $\hat{D}_{21} = 0$ at $C_2 = 0$ in both cases.

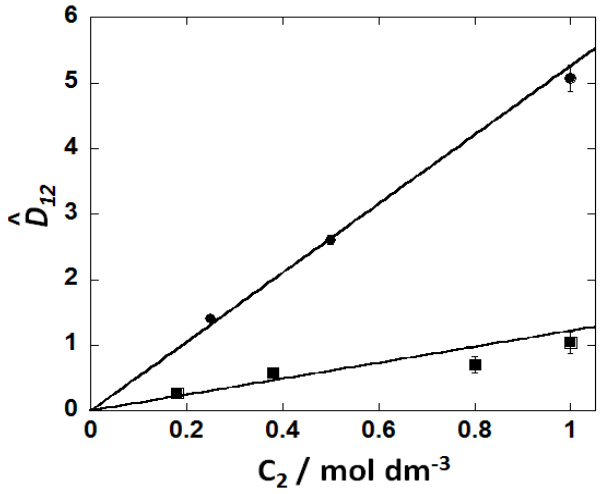

A)

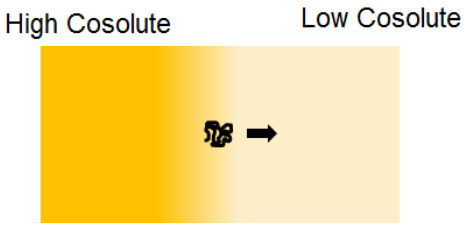

B)

Figure 4.2: A) Reduced Diffusiophoresis of PEG as a function of cosolute concentration, C_2 for the ternary PEG-TMAO-water (circles) and PEG-urea-water (squares) systems. B) Illustration showing PEG (coil) diffusiophoresis from high to low cosolute concentration (background color intensity).

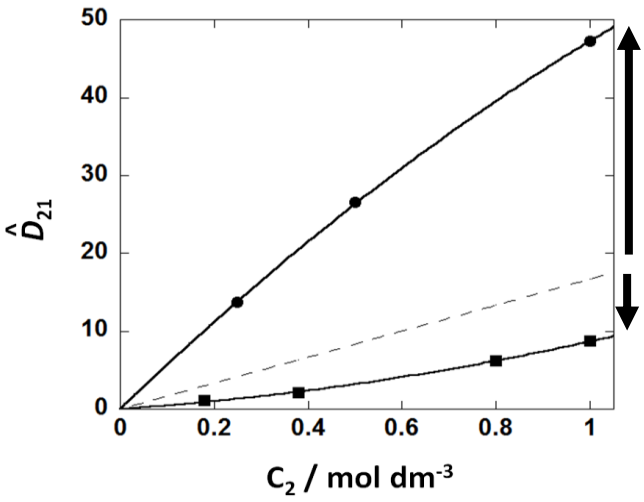

A)

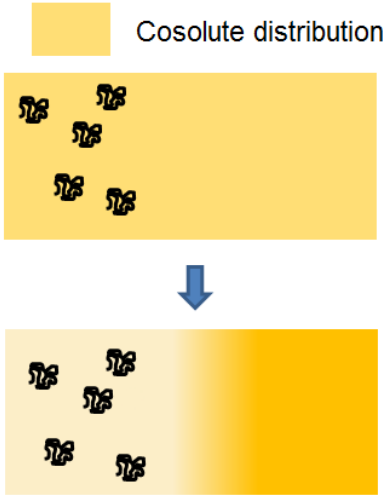

B)

Figure 4.3: A) Reduced cosolute osmotic diffusion as a function of cosolute concentration, C_2 for the ternary PEG-TMAO-water (circles) and PEG-urea-water (squares) systems. The plot of $\hat{D}_{21} = \bar{V}_1 C_2$ is included (dashed line). B) Illustration showing cosolute (background color intensity) osmotic diffusion from high to low PEG concentration (coils).

Interestingly, some curvature in the behavior of $\hat{D}_{21}(C_2)$ is observed at the higher cosolute experimental concentrations. Specifically, a downward curvature is observed in the TMAO case, while an upward curvature is observed in the urea case of $\hat{D}_{21}$.

Cosolute osmotic diffusion coefficient, compared to diffusiophoresis, has a more direct relation to thermodynamic interactions. In Fig. 4.3, we include the plot of $\hat{D}_{21} = \bar{V}_1 C_2$ (dashed line) for comparison, with $\bar{V}_1 = 16.7 \text{dm}^3 \cdot \text{mol}^{-1}$.[1] This line represents a baseline describing the predicted behavior of $\hat{D}_{21}(C_2)$ in the absence of polymer-cosolute net interactions (see Section 2.5). We can see that the $\hat{D}_{21}$ data obtained in the TMAO case are all above the baseline. On the other hand, the $\hat{D}_{21}$ data obtained in the urea case are all below the baseline. According to the excluded volume model (see section 2.5), our results imply that the polymer-TMAO net interactions and the polymer-urea net interactions are repulsive ($N_w > 0$) and attractive ($N_w < 0$), respectively. In the following section, we will first discuss the experimental behavior of $\hat{D}_{21}(C_2)$ in the framework of the excluded-volume (TMAO case) and ligand-binding (urea case) models. This analysis will provide the basis for understanding the experimental behavior of $\hat{D}_{12}(C_2)$.

Discussion

4.4 Examination of $\hat{D}_{21}$ and γ for the TMAO and urea cases

In this section, we determine γ and λ from the $\hat{D}_{12}$ and $\hat{D}_{21}$ data in Tables 4.7 and 4.8 at all the experimental cosolute concentrations. To determine these two parameters we rearrange Eqs. 2.18.1 and 2.18.2 in the following way:

$$\gamma = \frac{\hat{D}_{21} - \alpha \hat{D}_{12} - \bar{V}_1 C_2}{1-\alpha} \tag{4.6}$$

$$\lambda = \gamma - \hat{D}_{12} \tag{4.7}$$

In Tables 4.9 and 4.10 the calculated values of γ and λ are reported for the TMAO and urea cases, respectively. Note that the γ values were found to be positive in the TMAO case and negative in the urea case. The reported λ values will be examined in Section 4.4.3. In Fig. 4.4, we plot γ as a function of cosolute concentration for the TMAO and urea cases. Starting from $\gamma = 0$ at $C_2 = 0$, γ increases (decreases) as C_2 increases in the case of TMAO (urea). The slope of $\gamma(C_2)$ is related to the thermodynamic excess of water molecules according to Eq. 2.29.

In Tables 4.9 and 4.10, we also include the values of N_w obtained by using Eq. 2.29 (see section 2.5.1 on excluded-volume model, with $\bar{V}_0 = 0.01807\,\mathrm{dm^3 \cdot mol^{-1}}$). As we can see from Table 4.9, the values of N_w obtained in the TMAO case are all positive. Specifically an excess of ≈5 water molecules per PEG monomer (ethoxy group, -CH_2CH_2O-) is deduced by setting the number of PEG monomers to be 454 (based on the PEG molecular weight of 20 kg·mol^{-1}). As TMAO concentration increases, N_w reduces to ≈4 water molecules per ethoxy group. This effect can explained by considering a partial collapse of polymer due to osmotic stress exerted by the

TMAO molecules, which increases with the concentration of this osmolyte. In Table 4.9, we have also calculated the excluded volume and found that is about ≈3 fold larger than the polymer molar volume. These data allow us to conclude that strong repulsive interactions are observed between PEG and TMAO in water. It is important to appreciate that N_w was found to be ≈2 water molecules for PEG in the presence of chloride salts.[1] Thus, the TMAO "salting-out strength" is significantly higher than that observed for these salts.[1] The strong net PEG-TMAO repulsive interactions in water can be attributed to strong hydrogen bonds between TMAO and water. This is corroborated by infrared and raman spectroscopy studies.[64,65] For comparison, note that the largest value of $N_w = 7.8$ was obtained in the case of Na_2SO_4, consistent with the Hofmeister series.[1]

As we can see from Table 4.10, the values of N_w obtained in the urea case are all negative. Specifically a depletion of 1-2 water molecules per PEG monomer was observed. This implies that an excess of urea molecules is observed around the polymer chains. These findings will be quantitatively examined in the following section using a ligand-binding model.

Table 4.9: TMAO thermodynamic and kinetic values

C_2 / mol dm^{-3}	γ	λ	N_w *	$V_{ex} / \bar{V}_1$
0	0	0	(5.3)[a]	(3.60) [a]
0.25	10.0±0.2	8.6	4.9	3.39
0.5	19.0±0.3	16.4	4.6	3.28
1	31.6±0.1	26.6	3.9	2.89

* N_w values are reported for one monomer unit. There are 454 monomer units per polymer chain. [a] obtained by linear extrapolation.

Table 4.10: Urea thermodynamic and kinetic values

C_2 / mol dm^{-3}	γ	λ	N_w *
0	0	0	(-1.5) [a]
0.18	-2.0±0.2	-2.3	-1.4
0.38	-4.4±0.2	-5.0	-1.4
0.8	-7.4±0.2	-8.1	-1.1
1	-8.4±0.2	-9.4	-1.0

* N_w values are reported for one monomer unit. There are 454 monomer units per polymer chain. [a] obtained by linear extrapolation.

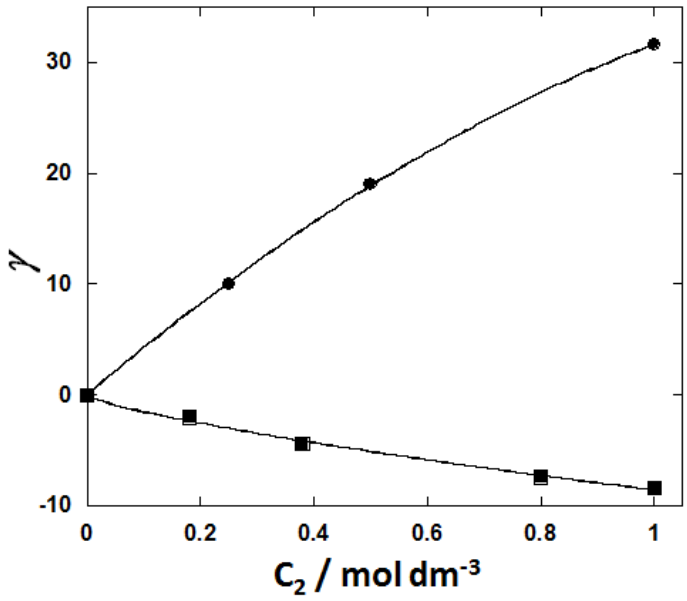

Figure 4.4: γ for TMAO(circles) and urea(squares) are reported here. Values of $\gamma > 0$ correspond to repulsion and $\gamma < 0$ corresponds to attraction between macromolecule and cosolute.

In conclusions, our experimental results show that the effects of TMAO and urea on PEG are in qualitative agreement with those observed in the case of proteins.[11] This suggests that the general trend of thermodynamic actions of TMAO, urea and salts does not depend on the type of macromolecules. We have also demonstrated that osmotic diffusion can be used to experimentally characterize thermodynamic interactions between macromolecules and cosolutes such as osmolyte and protein denaturants.

4.4.1 Examination of γ for the urea case based on ligand-binding models

In section 2.6, we have discussed macromolecule-ligand binding by introducing the Scatchard model (Eq. 2.34) and its generalization represented by the Hill model in order to account for cooperativity and anti-cooperativity effects. According to Eq. 2.34, the expression of γ for the Scatchard model is

$$\gamma = -\frac{n(C_2/K)}{1+(C_2/K)} \tag{4.8}$$

where n is the total number of sites on the host polymer and K is the PEG-urea dissociation constant. It is important to remember that this model assumes that the host binding sites are equivalent and independent. We fit our experimental values of γ in Table 4.10 based on Eq. 4.8, and obtain the values of $n = 21 \pm 3$ and $K/\mathrm{M} = 1.6 \pm 0.3$. Our results are shown in Figs. 4.5. The extracted value of n indicates that $454/21 = 22$ PEG monomeric units would be involved in a binding site. Since the size of a urea molecule ($60.06\,\mathrm{g \cdot mol^{-1}}$) is comparable with that of an ethoxy group ($46.07\,\mathrm{g \cdot mol^{-1}}$), we expect that a binding site would consist of one or two monomeric units at most. A possible mechanism of urea binding could involve hydrogen

bonding between the two amino groups of urea and two adjacent oxygen groups on the PEG chain. In this case, the total number of sites on the PEG chain would be $n = 227$.

Thus, it appears that $n \approx 20$ significantly underestimates the potential number of PEG binding sites. Since each monomeric unit can potentially serve as a binding site we set $n = 454$ in Eq. 4.8. In Fig. 4.6, the one-parameter fitting curve with $n = 454$ is shown. We can appreciate that this fitting curve significantly deviates from the experimental data. To examine how the deviation between experimental data and fitting curve depends on the value of n, we include in the same figure a one-parameter fitting curve obtained for $n = 57$, a value of n that is 8-fold smaller than the total number monomeric units. We can see from Fig. 4.6 that the deviation of the fitting curve from the experimental data remains quite large.

To explain the deviation of the experimental value of $\gamma(C_2)$ from the Scatchard model, we need to consider that the binding sites may not be equivalent and independent. It is possible that the peripheral sites on the PEG coil may be more prone to urea binding compared the internal PEG sites. Furthermore, urea binding to PEG may involve either one or two oxygens on the PEG chain. Finally, urea binding affinity towards PEG may decrease as PEG-urea binding progresses due to steric effects between two adjacent occupied sites. All these effects may be described as apparent or real anti-coperativity effects. Thus, under the previously-mentioned hypothesis that one urea molecule binds two adjacent monomeric units, we set $n = 227$ and examine our experimental data by using the expression of γ for the Hill model:

$$\gamma = -\frac{n(C_2 / K)^{n_H}}{1 + (C_2 / K)^{n_H}} \tag{4.9}$$

We fit our experimental values of γ in Table 4.10 based on Eq. 4.9 with $n = 227$, and obtain the values of $n_H = 0.77 \pm 0.04$ and $K / \mathrm{M} = 65 \pm 15$, consistent with binding anti-cooperativity.

Our results are shown in Fig. 4.7. The fitting curve shown in this figure is in satisfactory agreement with the experimental data. In conclusion, PEG-urea binding cannot be described by employing the Scatchard model because the obtained total number of binding sites is too small.

The Hill model satisfactorily describes the observed behavior of $\gamma(C_2)$ based on anti-cooperativity.

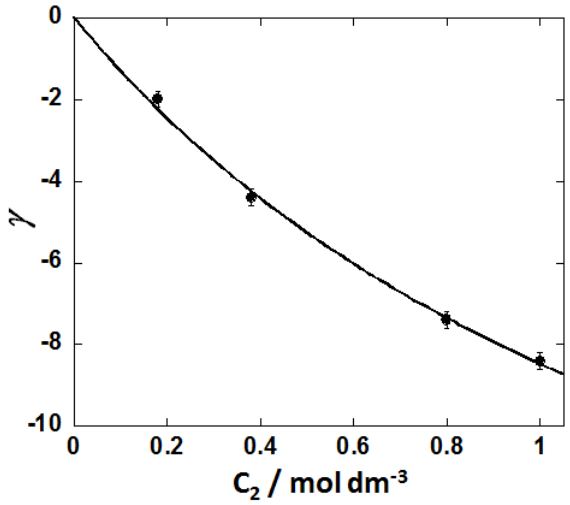

Figure 4.5: Thermodynamic parameter, γ, as a function of urea concentration, C_2. The solid curve is a fit through the data based on the two-parameter Scatchard model.

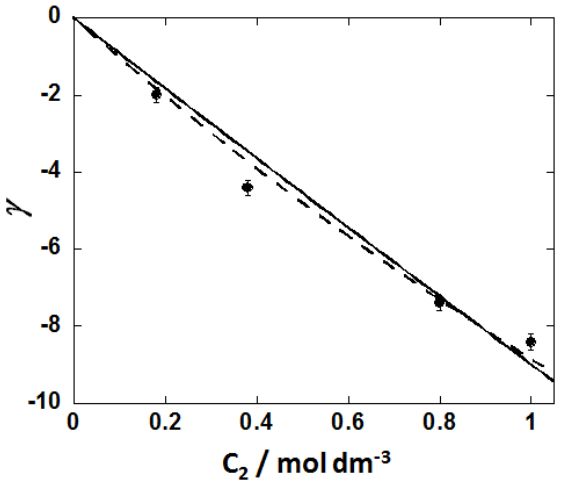

Figure 4.6: Thermodynamic parameter, γ, as a function of urea concentration, C_2. The two curves are a fit through the data based on the one-parameter Scatchard model with $n = 454$ (solid line) and $n = 57$ (dashed line).

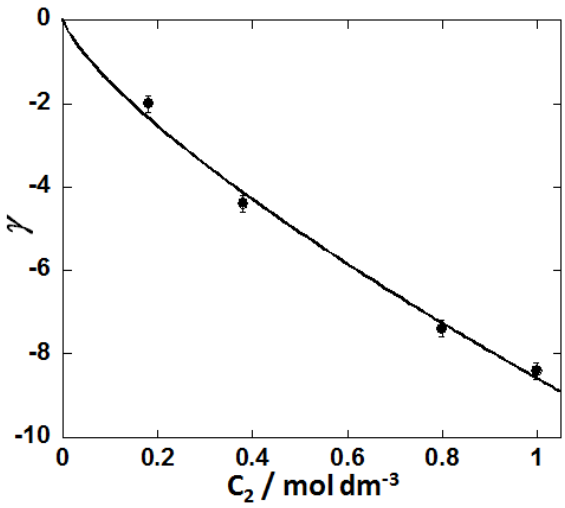

Figure 4.7: Thermodynamic parameter, γ, as a function of urea concentration, C_2. The solidcurve is a fit through the data based on the two-parameter Hill model with $n = 227$.

4.4.2 Examination of $\hat{D}_{12}$ for the TMAO case

Our experimental $\hat{D}_{12}$ values obtained in the TMAO case reveal that a concentration gradient of TMAO is responsible for a relatively large PEG diffusiophoresis, which we attribute to PEG-TMAO repulsive interactions in water. Similar behavior was observed for PEG in the presence of sodium sulfate concentration gradient. As in the case of salting-out agents, we examine our results according to Eq. 2.50 (in Section 2.8). According to this equation, $\hat{D}_{12}$ is directly proportional to the difference between the thermodynamic excess of water molecules (N_w) and the number of water molecules (n_w) diffusing with the hydrated macromolecule. After fitting the experimental values of $\hat{D}_{12}(C_2)$, we obtain: $N_w - n_w = 0.65 \pm 0.01$ per ethoxy unit. Based on $N_w = 5.3$, we then deduce that the ratio between bound and excess water molecules is $n_w / N_w = 0.88$.

It is important to remark that this value is the same as that obtained for PEG in the presence of salting out salts such as Na_2SO_4 and several chloride salts.[1] We have therefore found that n_w / N_w is independent of the precipitating strength of the cosolute for a given macromolecule.

4.4.3 Examination of $\hat{D}_{12}$ for the urea case

To describe the values of $\hat{D}_{12}$ obtained in the urea case, we derived a theoretical expression for the transport parameter λ based on urea binding. We start by writing transport linear law for each diffusing chemical species, *k*:

$$-J_k = \frac{C_k D_k}{RT} \nabla \mu_k \tag{4.10}$$

where J_k, C_k, D_k, and μ_k are the molar flux, molar concentration, tracer-diffusion coefficient and chemical potential of *k*, respectively. In our case, the chemical species are the free ligand, L, the free polymer, P and its complexes, PL_k, with $k = 1, 2, ..., n$. We assume that the cross-term Onsager transport coefficients describing the friction interaction between two chemical species can be neglected. We also assume that $D_{\mathrm{P}} = D_{\mathrm{PL}_k}$, because we expect that the binding of relatively small ligands have a marginal effect on the polymer hydrodynamic radius.

The macromolecule total flux, J_1, is the summation of the fluxes of all individual polymer species: $J_1 = J_{\mathrm{P}} + \sum_{k=1}^{n} J_{\mathrm{PL}_k}$. The macromolecule total flux is deduced from the mass balance:

$$-J_1 = \frac{D_{\mathrm{P}}}{RT}\left(C_{\mathrm{P}} \nabla \mu_{\mathrm{P}} + \sum_{k=1}^{n} C_{\mathrm{PL}_k} \nabla \mu_{\mathrm{PL}_k} \right) \tag{4.11}$$

The chemical-equilibrium condition: $\nabla\mu_{\mathrm{PL}_k} = \nabla\mu_{\mathrm{P}} + k\nabla\mu_{\mathrm{L}}$ allows us to write:

$$-J_1 = \frac{D_{\mathrm{P}}}{RT}\left(\sum_{k=0}^{n} C_{\mathrm{PL}_k}\nabla\mu_{\mathrm{P}} + \sum_{k=0}^{n} k\,C_{\mathrm{PL}_k}\nabla\mu_{\mathrm{L}}\right) \tag{4.12}$$

Since $\nabla\mu_1 = \nabla\mu_{\mathrm{P}}$ and $\nabla\mu_2 = \nabla\mu_{\mathrm{L}}$ and $\nu_{\mathrm{L}} \equiv \sum_{k=1}^{n} k\,C_{\mathrm{PL}_k} / C_1$, we finally obtain:

$$-J_1 = \frac{C_1 D_{\mathrm{P}}}{RT}\left(\nabla\mu_1 + \nu_{\mathrm{L}}\nabla\mu_2\right) \tag{4.13}$$

According to Eq. 2.12 ($-J_1 = L_{11}\nabla\mu_1 + L_{12}\nabla\mu_2$), we deduce from Eq. 4.13 that

$$\lambda = -\nu_{\mathrm{L}} \tag{4.14}$$

and

$$\hat{D}_{12} = 0 \tag{4.15}$$

This result implies that $\hat{D}_{12}$ for the PEG-urea-water system should be zero. Consistent with this model, we experimentally found that $\hat{D}_{12}$ in the urea case was significantly lower than that found in the TMAO case (see Fig. 4.2). However, the experimental values of $\hat{D}_{12}$ were not found to be negligible within the experimental error. Specifically, $\hat{D}_{12}(C_2)$ was found to slightly increase with C_2 starting from $\hat{D}_{12}(0) = 0$. In the remaining part of this section, we examine the the role of PEG-urea frictional interactions, which were neglected in the above model.

We want to identify an expression for λ based on frictional coefficients. We start from generalizing Eq. 4.14 by including the friction term in section 2.8:

$$\lambda = -\nu_{\mathrm{L}} - \frac{f_{12}}{f_{20}}\frac{C_2}{C_0} \tag{4.16}$$

According to Eqs. 4.14 and 2.42, we obtain:

$$\hat{D}_{12} = \frac{f_{12}}{f_{20}} \bar{V}_0 C_2 \tag{4.17}$$

According to Eq. 4.17, $\hat{D}_{12}$ is expected to increase with C_2 consistent with experimental findings. To quantitatively compare Eq. 4.17 with our experimental results, we first rewrite f_{12} / f_{20} in the following way:

$$\frac{f_{12}}{f_{20}} = \frac{f_{12}}{f_{10}} \frac{f_{10}}{f_{20}} = \frac{f_{12}}{f_{10}} \frac{D_2 / y_2}{D_1^0} = \frac{f_{12}}{f_{10}} \frac{1}{\alpha y_2} \tag{4.18}$$

where we have used Eq. 2.36 to link f_{10} to D_1^0 and f_{20} to D_2 / y_2. In Eq. 4.18, f_{12} describes the frictional interaction between polymer and cosolute, while f_{10} describes the frictional interaction between polymer and solvent.

We now hypothesize that the following relation between frictional coefficients and viscosities holds:

$$\frac{f_{1i}}{f_{1j}} = \frac{\eta_i}{\eta_j} \tag{4.19}$$

where f_{1i} is the coefficient describing the frictional interaction between the polymer and component i, and f_{1j} is the coefficient describing the frictional interaction between the polymer and component j. Correspondingly, η_i and η_j are the viscosities of pure components i and j, respectively. Our goal is to apply Eq. 4.19 to f_{12} / f_{10} in Eq. 4.18. For the solvent ($j = 0$ in Eq. 4.19), we can use the known viscosity of water, η_0. Since urea is solid, the viscosity of pure liquid urea is not experimentally accessible. However, measurements of viscosities on water-urea solutions were performed as a function of urea concentration (see Table 4.2). These data can be

used to extrapolate the hypothetical value of urea viscosity, η_2. Specifically, we write $\eta(C_2)$ as a weighted average between η_0 and η_2. We therefore write the following expression for the relative viscosity:

$$\eta_r = (1 - C_2\bar{V}_2) + C_2\bar{V}_2 \frac{\eta_2}{\eta_0} \tag{4.20}$$

where $C_2\bar{V}_2$ and $1 - C_2\bar{V}_2$ represents the volume fractions of urea and water, respectively. We fit the value of η_r in Table 4.2 according to Eq. 4.20 and determine $\eta_2 / \eta_0 = 1.92$. In Fig. 4.7, we plot the experimental values of $\hat{D}_{12}$ together with those predicted by applying Eqs. 4.17, 4.18 and $f_{12} / f_{10} = 1.92$ based on Eq. 4.19. We can see that our theoretical prediction is in good agreement with our experimental results. We therefore describe the observed behavior in the following way. Under a concentration gradient of urea, the flux of urea drags the polymer chains in the same direction of urea diffusion due to frictional interactions.

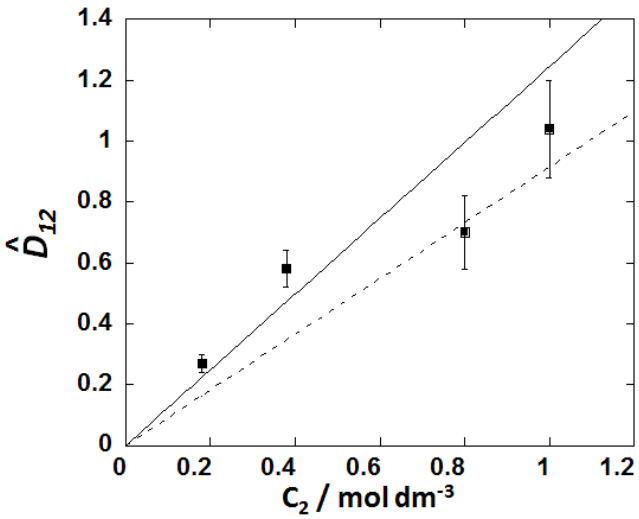

Figure 4.8: Reduced Diffusiophoresis of PEG as a function of cosolute concentration, C_2 for the ternary PEG-urea-water system. The solid line is a linear fit through the data. The dashed line is obtained from Eq. 4.17 with $f_{12} / f_{10} = 1.92$.

Chapter 5

Summary and Conclusions

5.1 Summary and Conclusion

We have characterized cosolute osmotic diffusion and polymer diffusiophoresis for PEG-TMAO-water and PEG-urea-water systems at 25 °C. We have successfully used our data of cosolute osmotic diffusion to characterize PEG-TMAO and PEG-urea thermodynamic interactions in water. The thermodynamic parameter, γ, was found to be positive in the TMAO case and negative in the urea case. This implies that PEG-TMAO and PEG-urea interactions are repulsive and attractive, respectively. Our thermodynamic results were described using the excluded-volume model (TMAO case) and the ligand-binding model (urea case). We conclude that the effect of TMAO and urea on PEG are comparable with those observed on proteins. This suggests that the macromolecule-TMAO and macromolecule-urea interactions do not significantly depend on the nature of the macromolecule.

PEG diffusiophoresis was found to occur from high to low cosolute concentration in both TMAO and urea cases. However, the magnitude of PEG diffusiophoresis in the case of TMAO was found to be significantly larger. Our diffusiophoresis results were described using a hydration model (TMAO case) and a friction model (urea case). We conclude that TMAO concentration gradients can be used to induce PEG diffusiophoresis more effectively than urea concentration gradients.

The mechanism of macromolecule diffusiophoresis from high to low TMAO concentration may play an important role in mass-transfer applications in which non-uniform TMAO concentrations are introduced. For example in Figure 5.1 (A), steady-state concentration gradients of TMAO could be exploited to drive the migration of macromolecules, with

applications similar to those of electrophoresis. Specifically, osmolyte concentration gradients could be used to achieve separation of two macromolecules with different diffusiophoresis properties. These type of applications are especially appealing in connection with microfluidic technologies. Furthermore in Fig. 5.1 (B), TMAO concentration gradients perpendicular to solid surfaces could be used to drive the migration of macromolecules towards the surface and catalyze their adsorption, with applications to coating and sensing technologies.

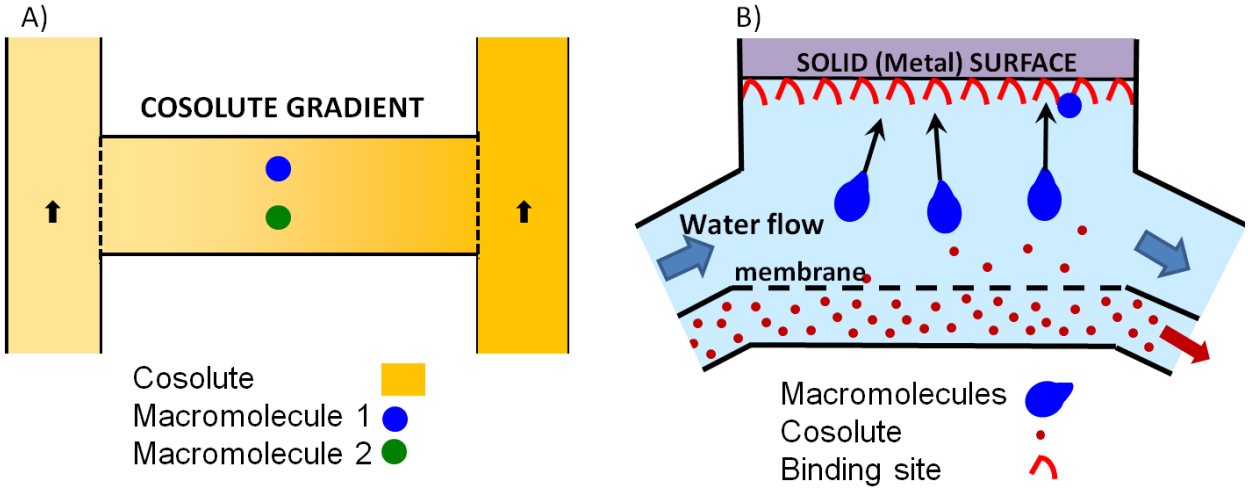

Figure 5.1: (A) Schematic apparatus for diffusiophoresis-induced separation of macromolecules. A mixture containing two macromolecules (1 and 2) is located inside a horizontal tube between two vertical reservoirs containing cosolute at different concentrations, thereby generating a cosolute concentration gradient inside the horizontal tube. The horizontal tube is separated from the reservoirs by two membranes not permeable to the macromolecules (dashed lines). The macromolecules are separated due to differences in their diffusiophoresis properties. (B) Schematic apparatus for diffusiophoresis-enhanced macromolecule adsorption. A flowing solution of macromolecules is in contanct with a solid surface (top) and a cosolute flowing solution (bottom). The macromolecule and cosolute solutions are separated by a membrane (dashed line).

Appendix A

Table A1: Binary diffusion experimental data for PEG 20K-water at 25°C

Experiment	1
$\bar{C}_1 / \text{mmol} \cdot \text{dm}^{-3}$	0.2500
$\Delta C_1 / \text{mol} \cdot \text{dm}^{-3}$	0.0004
$d_{bot} / \text{g} \cdot \text{cm}^{-3}$	0.998536
$d_{top} / \text{ g} \cdot \text{cm}^{-3}$	0.997210
J_{meas}	50.711
$D_A / 10^{-9} \text{m}^2 \cdot \text{s}^{-1}$	0.0584
$H_1 / \text{kg} \cdot \text{mol}^{-1}$	3.1222
$\bar{V}_0 / \text{dm}^3 \cdot \text{mol}^{-1}$	0.01811
$\bar{V}_1 / \text{dm}^3 \cdot \text{mol}^{-1}$	20.06

Table A2: Binary diffusion experimental data for TMAO-water at 25°C

Experiment	1	2	3
$\bar{C}_2 / \text{mol} \cdot \text{dm}^{-3}$	0.2500	0.5000	1.0000
$\Delta C_2 / \text{mol} \cdot \text{dm}^{-3}$	0.103113280	0.103078423	0.103424490
$d_{bot} / \text{ g} \cdot \text{cm}^{-3}$	0.9977292	0.9982654	0.9999181
$d_{top} / \text{ g} \cdot \text{cm}^{-3}$	0.9974552	0.9979795	0.9995195
J_{meas}	49.362	48.396	51.724
$D_A / 10^{-9} \text{m}^2 \cdot \text{s}^{-1}$	0.9102	0.9164	0.9300

Table A3: Binary diffusion experimental data for Urea-water at 25°C

Experiment	1	2	3	4
$\bar{C}_2 / \text{mol} \cdot \text{dm}^{-3}$	0.1800	0.3800	0.8000	1.0000
$\Delta C_2 / \text{mol} \cdot \text{dm}^{-3}$	0.126581797	0.126996772	0.128182286	0.126227706
$d_{bot} / \text{ g} \cdot \text{cm}^{-3}$	1.000942	1.004140	1.010802	1.0138903
$d_{top} / \text{ g} \cdot \text{cm}^{-3}$	0.998957	1.002051	1.008373	1.0119319
J_{meas}	49.442	50.033	47.949	50.012
$D_A / 10^{-9} \text{m}^2 \cdot \text{s}^{-1}$	1.368	1.352	1.321	1.308

Table A4: Ternary diffusion experimental data for 0.25 M TMAO and 0.2500 mM PEG

Experiment alpha reference file	1 0 TMPEt224	2 0 TMPEt223	3 1 TMPEt020	4 1 TMPEt210
$\bar{C}_1$ / mmol·dm^{-3}	0.2500	0.2500	0.2500	0.2500
$\bar{C}_2$ / mol·dm^{-3}	0.2500	0.2500	0.2500	0.2500
ΔC_1 / mol·dm^{-3}	0.0000	0.0000	0.0004	0.0004
ΔC_2 / mol·dm^{-3}	0.1005	0.1006	-0.0011	-0.0010
d_{bot} / g·cm^{-3}	0.998573	0.998569	0.999108	0.999106
d_{top} / g·cm^{-3}	0.998292	0.998279	0.997736	0.997753
J_{meas}	47.770	47.731	50.278	50.321
J_{calc}	47.740	47.761	50.286	50.313
D_A /10^{-9} m^2·s^{-1}	0.8671	0.8655	0.05794	0.05776

$\bar{\bar{C}}_1$ / mmol·dm^{-3}	0.2500	R_1 / dm^3·mol^{-1}	123715
$\bar{\bar{C}}_2$ / mol·dm^{-3}	0.2500	R_2 / dm^3·mol^{-1}	462
d_0 / g·cm^{-3}	0.9984308± 0.0000009		
H_1/kg·mol^{-1}	3.303±0.006		
H_2/kg·mol^{-1}	0.00244± 0.00003	$(D_{11})_v$ /10^{-9} m^2 s^{-1}	0.0548±0.0001
$\bar{V}_0$ / dm^3·mol^{-1}	18.07	$(D_{12})_v$ /10^{-12} m^2 s^{-1}	0.062±0.003
$\bar{V}_1$ / dm^3·mol^{-1}	16.75	$(D_{21})_v$ /10^{-9} m^2 s^{-1}	12.0±0.2
$\bar{V}_2$ / dm^3·mol^{-1}	0.10903	$(D_{22})_v$ /10^{-9} m^2 s^{-1}	0.892±0.002

Table A5: Ternary diffusion experimental data for 0.5 M TMAO and 0.2500 mM PEG

Experiment alpha reference file	1 0 TMPE0310	2 0 TMPE0317	3 1 TMPE0329	4 1 TMPE0323
$\bar{C}_1$ / mmol·dm^{-3}	0.2500	0.2500	0.2500	0.2500
$\bar{C}_2$ / mol·dm^{-3}	0.5000	0.5000	0.5000	0.5000
ΔC_1 / mol·dm^{-3}	0.0000	0.0000	0.0004	0.0004
ΔC_2 / mol·dm^{-3}	0.1005	0.1005	-0.0010	-0.0010
d_{bot} / g·cm^{-3}	0.999117	0.999151	0.999685	0.999650
d_{top} / g·cm^{-3}	0.998835	0.998817	0.998309	0.998279
J_{meas}	48.540	48.618	50.364	50.046
J_{calc}	48.580	48.578	50.209	50.202
D_A /10^{-9}m^2·s^{-1}	0.8755	0.8880	0.05830	0.05812

$\bar{\bar{C}}_1$ / mmol·dm^{-3}	0.2500	R_1 / dm^3·mol^{-1}	123439
$\bar{\bar{C}}_2$ / mol·dm^{-3}	0.5000	R_2 / dm^3·mol^{-1}	471
d_0 / g·cm^{-3}	0.9989803±0.000007		
H_1/kg·mol^{-1}	3.35±0.05		
H_2/kg·mol^{-1}	0.0027±0.0002	$(D_{11})_v$ /10^{-9} m^2 s^{-1}	0.0514±0.0001
$\bar{V}_0$ / dm^3·mol^{-1}	18.07	$(D_{12})_v$ /10^{-12} m^2 s^{-1}	0.058±0.002
$\bar{V}_1$ / dm^3·mol^{-1}	16.70	$(D_{21})_v$ /10^{-9} m^2 s^{-1}	23.6±0.3
$\bar{V}_2$ / dm^3·mol^{-1}	0.10879	$(D_{22})_v$ /10^{-9} m^2 s^{-1}	0.902±0.002

Table A6: Ternary diffusion experimental data for 1.0 M TMAO and 0.2500 mM PEG

Experiment alpha reference file	1 0 TMPG0913	2 0 TMPG0828	3 1 TMPE1018	4 1 TMPG1005
$\bar{C}_1$ / mmol·dm^{-3}	0.2500	0.2500	0.2500	0.2500
$\bar{C}_2$ / mol·dm^{-3}	1.000	1.000	1.000	1.000
ΔC_1 / mol·dm^{-3}	0.0000	0.0000	0.0004	0.0004
ΔC_2 / mol·dm^{-3}	0.1004	0.1006	-0.0011	-0.0009
d_{bot} / g·cm^{-3}	1.0008	1.0008	1.0012	1.0013
d_{top} / g·cm^{-3}	1.0005	1.0004	0.9999	0.9999
J_{meas}	52.883	52.836	51.013	51.054
J_{calc}	52.811	52.907	50.989	51.078
D_A /10^{-9} m^2·s^{-1}	0.8853	0.8886	0.05752	0.05783

$\bar{\bar{C}}_1$ / mmol·dm^{-3}	0.2500	R_1 / dm^3·mol^{-1}	125529
$\bar{\bar{C}}_2$ / mol·dm^{-3}	1.0000	R_2 / dm^3·mol^{-1}	513
d_0 / g·cm^{-3}	1.00057±0.00001		
H_1/kg·mol^{-1}	3.40± 0.06		
H_2/kg·mol^{-1}	0.0043±0.0003	$(D_{11})_v$ /10^{-9} m^2 s^{-1}	0.0444±0.0001
$\bar{V}_0$ / dm^3·mol^{-1}	18.08	$(D_{12})_v$ /10^{-12} m^2 s^{-1}	0.058±0.003
$\bar{V}_1$ / dm^3·mol^{-1}	16.68	$(D_{21})_v$ /10^{-9} m^2 s^{-1}	42.6±0.1
$\bar{V}_2$ / dm^3·mol^{-1}	0.10733	$(D_{22})_v$ /10^{-9} m^2 s^{-1}	0.914±0.002

Table A7: Ternary diffusion experimental data for 0.18 M Urea and 0.2500 mM PEG

Experiment alpha reference file	1 0 PUT6-16	2 0 PUT6-23	3 1 PUT6-8	4 1 PUT6-10
$\bar{C}_1 / \mathrm{mmol \cdot dm^{-3}}$	0.2500	0.2500	0.2500	0.2500
$\bar{C}_2 / \mathrm{mol \cdot dm^{-3}}$	0.1800	0.1800	0.1800	0.1800
$\Delta C_1 / \mathrm{mol \cdot dm^{-3}}$	0.0000	0.0000	0.0004	0.0004
$\Delta C_2 / \mathrm{mol \cdot dm^{-3}}$	0.1269	0.1268	0.0010	0.0009
$d_{bot} / \ \mathrm{g \cdot cm^{-3}}$	1.001715	1.001702	1.001371	1.001371
$d_{top} / \ \mathrm{g \cdot cm^{-3}}$	0.996046	0.996556	0.999912	0.999912
J_{meas}	49.740	49.874	50.395	50.300
J_{calc}	49.843	49.770	50.382	50.313
$D_A / 10^{-9} \mathrm{m^2 \cdot s^{-1}}$	1.340	1.341	0.0590	0.0587

$\bar{\bar{C}}_1 / \mathrm{mmol \cdot dm^{-3}}$	0.2500
$\bar{\bar{C}}_2 / \mathrm{mol \cdot dm^{-3}}$	0.1800
$R_1 / \mathrm{dm^3 \cdot mol^{-1}}$	123866
$R_2 / \mathrm{dm^3 \cdot mol^{-1}}$	392
$(D_{11})_v$ $/10^{-9}\ \mathrm{m^2\ s^{-1}}$	0.0578±0.0001
$(D_{12})_v$ $/10^{-12}\ \mathrm{m^2\ s^{-1}}$	0.005±0.002
$(D_{21})_v$ $/10^{-9}\ \mathrm{m^2\ s^{-1}}$	1.3±0.2
$(D_{22})_v$ $/10^{-9}\ \mathrm{m^2\ s^{-1}}$	1.346±0.001

Table A8: Ternary diffusion experimental data for 0.38 M Urea and 0.2500 mM PEG

Experiment alpha reference file	1 0 PUT7-28	2 0 PUT7-9	3 1 PUT7-24	4 1 PUT7-22
$\bar{C}_1$ / mmol·dm^{-3}	0.2500	0.2500	0.2500	0.2500
$\bar{C}_2$ / mol·dm^{-3}	0.3800	0.3800	0.3800	0.3800
ΔC_1 / mol·dm^{-3}	0.0000	0.0000	0.0004	0.0004
ΔC_2 / mol·dm^{-3}	0.1281	0.1279	0.0009	0.0011
d_{bot} / g·cm^{-3}	1.004969	1.004969	1.004587	1.004602
d_{top} / g·cm^{-3}	0.999414	0.999415	1.003015	1.003226
J_{meas}	49.886	49.868	50.095	50.130
J_{calc}	49.909	49.845	50.085	50.140
D_A /10^{-9} m^2·s^{-1}	1.321	1.326	0.0587	0.0588

$\bar{\bar{C}}_1$ / mmol·dm^{-3}	0.2500
$\bar{\bar{C}}_2$ / mol·dm^{-3}	0.3800
R_1 / dm^3·mol^{-1}	123303
R_2 / dm^3·mol^{-1}	389
$(D_{11})_v$ /10^{-9} m^2 s^{-1}	0.0574±0.0001
$(D_{12})_v$ /10^{-12} m^2 s^{-1}	0.005±0.002
$(D_{21})_v$ /10^{-9} m^2 s^{-1}	2.5±0.2
$(D_{22})_v$ /10^{-9} m^2 s^{-1}	1.328±0.001

Table A9: Ternary diffusion experimental data for 0.8 M Urea and 0.2500 mM PEG

Experiment alpha reference file	1 0 PUT9-23	2 0 PUTT1027	3 1 PUTT10-5	4 1 PUTT10-9
$\bar{C}_1$ / mmol·dm^{-3}	0.2500	0.2500	0.2500	0.2500
$\bar{C}_2$ / mol·dm^{-3}	0.8000	0.8000	0.8000	0.8000
ΔC_1 / mol·dm^{-3}	0.0000	0.0000	0.0004	0.0004
ΔC_2 / mol·dm^{-3}	0.1267	0.1265	0.0007	0.0007
d_{bot} / g·cm^{-3}	1.011591	1.010907	1.010712	1.010976
d_{top} / g·cm^{-3}	1.009420	1.009472	1.009563	1.009999
J_{meas}	49.664	49.710	50.155	50.201
J_{calc}	49.710	49.664	50.172	50.183
D_A /10^{-9} m^2·s^{-1}	1.292	1.290	0.05875	0.05887

$\bar{\bar{C}}_1$ / mmol·dm^{-3}	0.2500
$\bar{\bar{C}}_2$ / mol·dm^{-3}	0.8000
R_1 / dm^3·mol^{-1}	123793
R_2 / dm^3·mol^{-1}	392
$(D_{11})_v$ /10^{-9} m^2 s^{-1}	0.0564±0.0001
$(D_{12})_v$ /10^{-12} m^2 s^{-1}	-0.004±0.002
$(D_{21})_v$ /10^{-9} m^2 s^{-1}	7.4±0.2
$(D_{22})_v$ /10^{-9} m^2 s^{-1}	1.299±0.001

Table A10: Ternary diffusion experimental data for 1.0 M Urea and 0.2500 mM PEG

Experiment alpha reference file	1 0 04-06-14	2 0 03-16-14	3 1 03-09-14	4 1 03-23-14
$\bar{C}_1 / \text{mmol} \cdot \text{dm}^{-3}$	0.2500	0.2500	0.2500	0.2500
$\bar{C}_2 / \text{mol} \cdot \text{dm}^{-3}$	1.0000	1.0000	1.0000	1.0000
$\Delta C_1 / \text{mol} \cdot \text{dm}^{-3}$	0.0000	0.0000	0.0004	0.0004
$\Delta C_2 / \text{mol} \cdot \text{dm}^{-3}$	0.1254	0.1254	0.0000	0.0001
$d_{bot} / \ \text{g} \cdot \text{cm}^{-3}$	1.014941	1.014698	1.014348	1.014372
$d_{top} / \ \text{g} \cdot \text{cm}^{-3}$	1.012681	1.012712	1.013045	1.012973
J_{meas}	49.169	49.607	49.723	49.800
J_{calc}	49.163	49.613	49.743	49.779
$D_A / 10^{-9} \text{m}^2 \cdot \text{s}^{-1}$	1.280	1.280	0.05827	0.05800

$\bar{\bar{C}}_1 / \text{mmol} \cdot \text{dm}^{-3}$	0.2500	$R_1 / \text{dm}^3 \cdot \text{mol}^{-1}$	122376
$\bar{\bar{C}}_2 / \text{mol} \cdot \text{dm}^{-3}$	1.0000	$R_2 / \text{dm}^3 \cdot \text{mol}^{-1}$	392
$d_0 / \ \text{g} \cdot \text{cm}^{-3}$	1.1367±0.0063		
$H_1 / \text{kg} \cdot \text{mol}^{-1}$	3.4370± 0.3933		
$H_2 / \text{kg} \cdot \text{mol}^{-1}$	0.016754± 0.000892	$(D_{11})_v$ $/10^{-9}$ m^2 s^{-1}	0.0558±0.0001
$\bar{V}_0 / \text{dm}^3 \cdot \text{mol}^{-1}$	18.07	$(D_{12})_v$ $/10^{-12}$ m^2 s^{-1}	-0.002±0.002
$\bar{V}_1 / \text{dm}^3 \cdot \text{mol}^{-1}$	14.80	$(D_{21})_v$ $/10^{-9}$ m^2 s^{-1}	9.3±0.4
$\bar{V}_2 / \text{dm}^3 \cdot \text{mol}^{-1}$	0.84334	$(D_{22})_v$ $/10^{-9}$ m^2 s^{-1}	1.285±0.002

Bibliography

[1] McAfee, M.S.; Zhang, H.; Annunziata, O. *Langmuir,* **2014,** *30,* 12210-12218.

[2] Bird, R. B. *AIChE J*. **2003**, *50*, 273−287.

[3] Curtiss, C. F.; Bird, R. B. *Ind. Eng. Chem. Res.* **1999**, *38*, 2515−2522.

[4] Tyrrell, H. J. V.; Harris, K. R. *Diffusion in Liquids*; Butterworths: London, 1984.

[5] Dror, I.; Amitay, T.; Yaron, B.; Berkowitz, B. *Science* **2003**, *300,* 950.

[6] Schurr, J. M.; Fujimoto, B. S.; Huynh, L.; Chiu, D. T. *J. Phys. Chem. B* **2013**, *117*, 7626−7652.

[7] Patterson, G. *Physical Chemistry of Macromolecules,* CRC Press: U.S. **2007.**

[8] McAfee, M.S.; Annunziata, O. *Langmuir,* **2015,** *31*, 1353-1361.

[9] Annunziata, O.; Buzatu, D.; Albright, J. G. *J. Phys. Chem. B.* **2012**, *116*, 12694−12705.

[10] McAfee, M. S.; Annunziata, O. *Langmuir* **2012,** *30*, 4916−4923.

[11] Arakawa, T.; Timasheff, S. N. *Biochemistry* **1982**, *21*, 6545−6552.

[12] Tan, C.; Albright, J. G.; Annunziata, O. *J. Phys. Chem. B* **2008**, *112*, 4967−4974.

[13] Annunziata, O. Analysis of the Protein-Salt Coupled Transport. Ph.D. thesis, Texas Christian University, 2001.

[14] Beard, Daniel A. Qian, H. *Chemical Biophysics*, Cambridge Univ. Press: U.K., 2008.

[15] Prieve, D. C. *Adv. Coll. Interface Sci.* **1982,** *16*, 321−335.

[16] Abecassis, B.; Cottin-Bizonne, C.; Ybert, C.; Ajdari, A.; *Nat. Mater.* **2008,** *7*, 785−789.

[17] Palacci, J.; Abecassis, B.; Cottin-Bizonne, C.; Ybert, C.; Bocquet,́ L; *Phys. Rev. Lett*. **2010,** *104*, 138302.

[18] Velegol, D.; Garg, A.; Guha, R.i; Kar, A.; Kumar, M. *Roy. Soc. Ch.* **2016,** *12*, 4686.

[19] Tang, G.D.; Yan, C.; Yang, H.; Gong, J.; Chai, C., Lam, Y.C. *Electrophoresis*, **2006**, *27*, 628-639.

[20] Abecassis, B.; Cottin-Bizonne, C.; Ybert, C.; Ajdari, A.; Bocquet,́ L. *New J. Phys.* **2009**, *11*, 075022.

[21] Florea, D.; Sami Musaa, S.; Huyghea, J. M. R.; Wyss, H. M. *Proc. Natl. Acad. Sci. U.S.A.* **2014**, *111*, 6554−6559.

[22] Liu, X.; Vlugt, T. J. H.; Bardow, A. *Ind. Eng. Chem*. Res. **2011**, *50*, 10350–10358.

[23] Zhang, H.; Annunziata, O. *Phys. Chem. Chem. Phys*., **2009**, 8923–8932.

[24] Tan, C.; Albright, J. G.; Annunziata, O. *J. Phys. Chem.B*, **2008**, *112*, 4967-4974.

[25] McAfee, Michele S. Polymer Migration Induced by Concentration Gradients of Salts or Crowding Agents. Ph.D. thesis, Texas Christian University, 2014.

[26] Kim, P. *Nanotechnology*, **2005**, *16*, 2420.

[27] Lin, C. C.; Anseth, K. S. *Pharmaceutical Research*, **2009,** 26, 631-643.

[28] Albertsson, P. A. *Partition of Cell Particles and Macromolecules*; Wiley: New York, 1986.

[29] McPherson, A. *Crystallization of Biological Macromolecules*; Cold Spring Harbor: New York, 1998.e. 2009.

[30] Arakawa, T.; Bhat, R.; and Timasheff, S. N. *Biochemistry*, **1990**, *29*, 1914–1923.

[31] Timasheff, S. N. *Adv. Protein Chem.*, **1998**, *51*, 355–432.

[32] Timasheff, S. N. *Biochemistry*, **2002**, 41, 13473–13482.

[33] Zhang, Y.; Cremer, P. *Annu. Rev. Phys. Chem.*, **2010**, *61*, 63-83.

[34] Deepak R.; Jayasimha, P.; Rau, D.C.; Makhatadze, G.I.; Garcia, A. E. *J. Phys. Chem.*, **2012**, *40*, 12095-12104.

[35] Einstein, A. *Ann. Phys*. **1905**, *17*, 549–560.

[36] Stokes, G. G. *Trans. Cambridge Philos. Soc*. **1850**, *9*, 8.

[37] Krishna, R.; Wesselingh, J. A. *Chem. Eng. Sci*. **1997**, *52*, 861–911.

[38] Kirkwood, J. G.; Baldwin, R. L.; Dunlop, P. J.; Gosting, L. J.; Kegeles, G. *J. Chem. Phys.* **1960**, *33*, 1505.

[39] Dunlop, P. J.; Gosting, L. J. *J. Phys. Chem.* **1959**, *63*, 86–93.

[40] Miller, D. G. *J. Phys. Chem.* **1986**, *90*, 1509–1519.

[41] Rard, J. A.; Miller, D. G. *J. Sol. Chem.* **1979**, *8*, 755−766.

[42] Rard, J. A.; Clegg, S. L.; Palmer, D. A. *J. Sol. Chem.* **2000**, *29*, 1−49.

[43] Miller, D. G.; Albright, J. G. *Optical methods. In Measurement of the Transport Properties of Fluids: (Experimental Thermodynamics)*; Wakeham, W. A., Nagashima, A., Sengers, J., Eds.; 1991; Vol. III; pp 272−294.

[44] Miller, D. G.; Vitagliano, V.; Sartorio, R. *Langmuir* **2014**, *30*, 12210−12219.

[45] Miller, D. G. *J. Phys. Chem.* **1988**, *92*, 4222−4226.

[46] Gosting, L. J. *Adv. Protein Chem.;* 1956; pp 429–554.

[47] Baldwin, R. L.; Dunlop, P. J.; Gosting, L. J. *J. Am. Chem. Soc*. **1955**, *77*, 5235–5238.

[48] Fujita, H.; Gosting, L. J. *J. Am. Chem. Soc*. **1956**, *78*, 1099–1106.

[49] Rard, J. A.; Miller, D. G. *J. Solution Chem.* **1979**, *8*, 755–766.

[50] Gosting, L. J.; Kim, H.; Loewenstein, M. A.; Reinfelds, G.; Revzin, A. *Rev. Sci. Instrum.* **1973**, *44*, 1602.

[51] Miller, D. G.; Albright, J. G.; Mathew, R.; Lee, C. M.; Rard, J. A.; Eppstein, L. B. *J. Phys. Chem.* **1993**, *97*, 3885–3899.

[52] Gosting, L. J.; Kim, H.; Loewenstein, M. A.; Reinfelds, G.; Revzin, A. *Rev. Sci. Instrum*. **1973**, *44*, 1602.

[53] Vanag, V. K.; Epstein, I. R. *Phys. Chem. Chem. Phys*. **2009**, *11*, 897–912.

[54] Albright, J. G.; Annunziata, O.; Miller, D. G.; Paduano, L.; Pearlstein, A. J. *J. Am. Chem. Soc.* **1999**, *121*, 3256–3266.

[55] Rard, J. A.; Miller, D. G. *J. Chem. Eng. Data* **1980**, *25*, 211–215.

[56] Chanchi, R. D.; Jayasimha,P.; Rau, D.C.; Makhatadze, G.I.; Garcia, A.E. *J. Phys. Chem. B,* **2012**, *116*, 12095-12104.

[57] Dmitriy M.; Egorov, G.; Kolker, A. *J. Chem. Eng. Data*, **2015**, *60*, 1291−1299.

[58] Sinibaldi, R.; Casieri, C.; Melchionna, S., Onori, G.; Segre, A. L.; Viel, S.; Mannina, L.; De Luca, F. *J. Phys. Chem. B*, **2006**, *110*, 8885-8892.

[59] Ellerton, H.D.; Dunlop, P.**,** *J. Phys. Chem.*, **1966**, *70*. (6), 1831–1837.

[60] Hamilton, D.; Stokes, R.H., *J. Sol. Chem.* **1972**, *1*, 213-221.

[61] Kawahara, K.; Tanford, C. *J. Biol. Chem.***1966**, *231*, 3228-3232.

[62] Record, M. T.; Anderson, C. F. *Biophys. J.* **1995**, *68*, 786–794.

[63] Tanford, C. *Physical Chemistry of Macromolecules*; Wiley: New York, 1967; p 356.

[64] Panuszko; Bruzdziak, P.; Zielkiewicz J.; Wyrzykowski, D.; Stangret, J. *J. Phys. Chem. B* **2009**, *113*,14797-14809.

[65] Knake, L.; Schwaab, G.; Kartaschew, K.; Havenith, M. *J. Phys. Chem. B* **2015**, *119*, 13842-13851.

[66] Annunziata, O.; Buzatu, D.; Albright, J. G. *Langmuir* **2005**, *21*, 12085− 12089.

[67] Zhang, H.; Annunziata, O. *J. Phys. Chem. B* **2008**, *112*, 3633−3643

Vita

Lara Richelle Lechlitner was born on November 1, 1987 in Fort Worth, Tx. She is the daughter of Larry Williams, Pharm. D. and Vickie Williams, an educator. After graduating Venus High School in Venus, Tx, 2006, she received a Bachelor of Science degree in Chemistry with interdisciplinary studies in Biology from Tarleton State University in Stephenville, Tx in 2011.

With a degree from Tarleton State University, she obtained a Texas Teaching certificate and taught Chemistry at West High School in West, Tx. She worked in West for two years, leading the science club and serving as secretary for the Association of Texas Professional Educators for the high school campus.

In August 2014, she became a full-time graduate school at Texas Christian University. While working on graduate studies in Physical Chemistry under Dr. Onofrio Annunziata, she served as laboratory teaching assistant for three semesters.

She currently resides in Burleson, Texas. Married to her husband John Lechlitner for three years, they have one child, Lily Elizabeth Lechlitner.

Abstract

DIFFUSIOPHORESIS AND OSMOTIC DIFFUSION IN TERNARY AQUEOUS MIXTURES OF POLYETHYLENE GLYCOL CONTAINING TRIMETHYLAMINE-N-OXIDE OR UREA AS COSOLUTES

By Lara Richelle Lechlitner, MS, 2017
Department of Chemistry amd Biochemistry
Texas Christian University

Thesis Advisor: Onofrio Annunziata, Professor of Chemistry

Diffusiophoresis is the net migration of macromolecules within liquid mixtures induced by a concentration gradient of a cosolute. Osmotic diffusion is the net migration of cosolute molecules induced by a concentration gradient of a macromolecules. The diffusiophoresis of polyethylene glycol (PEG) induced by cosolute concentration gradients were experimentally characterized together with cosolute osmotic diffusion by Rayleigh Interferometry at 25°C. In this investigation, trimethylamine-N-oxide (TMAO) and urea were chosen as two distinct cosolute cases inspired by their opposite applications in protein aqueous systems. Our results on cosolute osmotic diffusion were successfully used to characterize the PEG-TMAO (repulsive) and PEG-urea (attractive) net interactions in water. Moreover, PEG diffusiophoresis in the TMAO case was found to be five-fold larger than that observed in the urea case. This suggests that TMAO concentration gradients could be exploited to induce the migration of macromolecules with applications in the fields of separation, adsorption and microfluidic technologies.